Exploring the mechanisms underlying the phenotype of MCAD deficiency with Systems Medicine

Martines, Anne-Claire

Chapter 5

Simulating the impact of genetic and environmental modifiers on MCAD deficiency in an extended computational model of human liver fatty-acid catabolism

Anne-Claire M.F. Martines[1,#], Dirk-Jan Reijngoud[1,2], Barbara M. Bakker[r1,‡]

[1] Laboratory of Pediatrics, Center of Liver, Digestive and Metabolic Diseases, University of Groningen, Groningen, University Medical Center Groningen, Groningen, The Netherlands,
[2] Department of Analytical Biochemistry, University of Groningen, Groningen, The Netherlands.

Abstract

Mitochondrial fatty-acid beta-oxidation (mFAO) in the liver is of critical importance for energy metabolism during fasting and under other energy-demanding conditions. Chapters 3 and 4 have shown the importance of surrounding pathways and peripheral tissues on hepatic mFAO function in MCAD deficiency. In this study, we used computational modeling to gain more insight into the role of the surrounding network on mFAO function in MCAD deficiency. To this end, we humanized the rat dynamic model of the mFAO pathway and extended it with relevant pathways of energy and detoxification metabolism. The simulated fluxes and metabolite profiles reflect the relative disease severities of SCAD, MCAD, and VLCAD deficiency in humans. Furthermore, we simulated changes in the surrounding network, including that of the futile cycle of acyl-CoA hydrolysis and reactivation. Repression of this cycle by modulating the substrate specificity of CPT1, impaired the mFAO flux in the MCAD deficient model, but hardly in the VLCAD or SCAD deficient models. These results give a first indication how differences in genetic background related to the surrounding pathways could affect the vulnerability of MCADD patients to metabolic crisis.

Introduction

Mitochondrial fatty acid beta-oxidation (mFAO) in the liver is of key importance for energy homeostasis during fasting or conditions of high energy demand. In the cell, fatty acids are first activated by formation of a fatty-acid-coenzyme A (CoA) ester (acyl-CoA) in the cytosol. The resulting cytosolic acyl-CoA esters are taken up into the mitochondria and oxidized to acetyl-CoA, which is further oxidized in the citric acid cycle for the formation of ATP. In addition, the liver can convert acetyl-CoA to ketone bodies, which are used by peripheral tissues during fasting, thus saving glucose.

The fatty-acid beta-oxidation starts with the transport of the acyl-chain of cytosolic acyl-CoA into mitochondria by the carnitine-shuttle (**Figure 1**, with the shuttle enzymes given in green). This shuttle comprises three consecutive reactions, transfer of the acyl chain from acyl-CoA onto carnitine catalyzed by carnitine palmitoyltransferase (CPT)1, transport of acyl-carnitine across the mitochondrial inner membrane in exchange for carnitine by carnitine acyl-carnitine transporter (CACT), and transfer of the acyl chain from acyl-carnitine onto CoASH by CPT2. Next this acyl-CoA is shortened in repetitive four-reaction cycles, thereby producing an acetyl-CoA molecule [1–3] in each cycle. The first reaction in each cycle is catalyzed by a set of isoenzymes, which accept a range of acyl-CoA substrates of different, overlapping carbon-chain lengths. In humans, these are very-long-, medium-, and short-chain acyl-CoA dehydrogenase (VLCAD, MCAD, and SCAD) [3,4]. In this reaction, acyl-CoA is dehydrogenated, forming enoyl-CoA, and FAD bound in the acyl-CoA dehydrogenase is reduced to $FADH_2$. The reducing equivalents are subsequently transferred to the protein electron transfer flavoprotein (ETF) and finally to ETF dehydrogenase (*i.e.* ETF ubiquininone oxidoreductase ETFQO) transfers the reducing equivalents from ETF-bound $FADH_2$ to CoQ in the mitochondrial electron transport chain. In three consecutive reactions, enoyl-CoA is hydrated, again dehydrogenated, thereby reducing NAD^+ to NADH, and finally thiolyzed. The thiolase reaction produces a shortened acyl-CoA ester and acetyl-CoA, with the concomitant consumption of a free CoA molecule (referred to as CoASH, because of its free thiol group). The products of mFAO, acetyl-CoA, NADH and acyl-CoA-dehydrogenase-bound $FADH_2$, can be further oxidized to produce ATP in the tricarboxylic acid (TCA) cycle and oxidative phosphorylation (OXPHOS). During fasting or intense exercise, the liver uses this ATP for the production of glucose by gluconeogenesis.

Inborn deficiencies associated with human disease have been identified for almost all the mFAO enzymes [3,5]. Under energy-demanding conditions, individuals with an mFAO deficiency run a risk of severe, life-threatening hypoketotic hypoglycemia. Since the isoenzymes VLCAD, MCAD, and SCAD have overlapping substrate specificities [3,4], they can in principle take over each other's role. This may explain why SCAD-deficient (SCADD) children often have only minor symptoms [6]. The disease presentation generally becomes more severe from SCADD to MCADD to VLCADD [3]. However, there is a large heterogeneity in disease presentation between mFAO-deficient (mFAOD) individuals with the same enzyme deficiency, and even with the same genetic mutation. For example, a subset of children with a homozygous loss-of-function c.985A>G mutation in the *ACADM* gene, which encodes MCAD, can present with life-threatening hypoglycemia[3,5], while a different subset of these children never develops any symptoms [7–15]. It was reported that individuals homozygous for the c.985A>G mutation are able to fast for 18-24 hours [3,7,16,17]. A combination of prolonged fasting and an additional trigger, such as an airway

or gastrointestinal infection, alcohol use, or cold-exposure, increases the risk of hypoketotic hypoglycemia [5,15,18–20].

To investigate the biochemical basis for the difference in metabolic robustness between individuals, we have constructed a dynamic computational model of the mFAO[26]. Model simulations revealed a potential vicious cycle of CoA ester accumulation, CoASH depletion, and mFAO flux decline [21], which was caused by a high concentration of the substrate palmitoyl-CoA and aggravated by loss of MCAD [4]. The CoASH-consuming enzyme of the last mFAO reaction, medium-chain ketoacyl-CoA thiolase (MCKAT) and the NAD^+-reducing enzyme medium-chain hydroxyacyl-CoA dehydrogenase (MSCHAD) played an important role in the underlying mechanism [21] (**Chapter 2**). The model was based on biochemical data that had been collected mostly from rat mitochondria. A human version of the model has been derived by fitting of a subset of model parameters to plasma acyl-carnitines of healthy individuals [22]. This human model version could explain the difference in severity of disease presentation between two individuals with multiple-acyl-CoA dehydrogenase deficiency (MADD), a condition caused by a defect in ETF or ETF dehydrogenase [22]. The model has however, not yet been applied to investigate heterogeneous disease presentation of other enzyme defects.

Potentially, subtle differences in genetic background explain differences in vulnerability of robustness of mFAO patients. This may be related to differences within the mFAO pathway, e.g. due to differences in concentrations or activity of the remaining enzymes. However, the cofactors NAD^+ and CoASH availability also plays a critical role in mFAO. Therefore, we looked into the intricate connection of the mFAO pathway with other metabolic pathways of metabolism, particularly those in which these cofactors are involved. Since a high mFAO flux requires high concentrations of NAD^+ and CoASH, we hypothesize that pathways that increase these concentrations, may alleviate clinical symptoms. In contrast, pathways that decrease NAD^+ or CoASH, may aggravate the risk of a metabolic crisis.

The pathways that utilize the products of mFAO are typically in the category of alleviating pathways. In this category, ketogenesis is the production of the ketone bodies β-hydroxy-butyrate and acetoacetate in the liver (**Figure 1**). These ketone bodies are secreted into the plasma for consumption as fuel by peripheral tissues and brain. The ketogenesis pathway uses acetyl-CoA and acetoacetyl-CoA (C4-ketoacyl-CoA) as substrates and regenerates CoASH. In the conversion of acetoacetate to β-hydroxy-butyrate (roughly 25-48% of the total ketone-body pool [23,24]), NADH is reoxidized into NAD^+. By increasing both CoASH and NAD^+, the ketogenesis pathway should stimulate the mFAO flux. Second, the OXPHOS system is the major ATP-producing system that reoxidizes NADH to NAD^+ and protein-bound $FADH_2$ to FAD^+. An active OXPHOS pathway would therefore stimulate the mFAO. Recently, however, it was reported that the OXPHOS system functions suboptimally in fibroblasts of MCADD patients [25], which might aggravate their clinical symptoms [4,26]. Third, the export of acyl-carnitines can relieve the mitochondria from accumulating CoA esters and thereby liberate CoASH. Finally, the hydrolysis of acyl-CoA esters by mitochondrial acyl-CoA thioesterases (ACOT) releases CoASH and may thereby stimulate the mFAO. The resulting free fatty acids (FFAs) may be secreted and reactivated by cytosolic acyl-CoA synthetases (ACSs) (**Figure 1**). This futile cycle has indeed been reported to contribute to the mFAO flux [27–30] and may therefore alleviate disease symptoms. The final alleviating pathway would be the microsomal ω-oxidation pathway, which oxidizes

medium-chain fatty acids to their corresponding dicarboxylic acids. This pathway would be a sink for medium-chain acyl-CoA esters that tend to accumulate when MCAD is deficient. Indeed, MCADD individuals show higher medium-chain dicarboxylic acid levels in blood and urine compared to unaffected individuals, indicating that the omega-oxidation can be considered a potential rescue pathway in mFAOD [31]. According to our rationale, processes that compete for the available CoASH or NAD^+ would inhibit the mFAO and may aggravate the risk of clinical symptoms [32,33]. Simultaneous oxidation of multiple substrates would be in this category. During fasting, oxidation of glucose should be minimal. Breakdown of proteins, however, would produce higher levels of amino acids. Particularly the catabolism of branched-chain amino acids requires CoASH. In addition, catabolism of xenobiotics requires CoASH.

The aim of this study was to explore the impact of potential alleviating pathways on the hepatic mFAO flux, in order to gain insight into mechanisms underlying the disease presentation of VLCADD, MCADD and SCADD. To this end, we revisited the conversion of the rat mFAO model into a human version, and extended it with the alleviating pathways discussed above. Co-catabolism of competing substrates is not part of this study. In the extended model we simulated deficiencies of the different acyl-CoA dehydrogenases (ACADs) and made subtle variations in cofactor availabilities or activities of the added pathways. We show that the model reproduces the differences in disease severity that are generally observed between VLCADD, MCADD, and SCADD patients. In addition, the simulated interventions show that differences in cofactor availability and enzyme activities may give rise to different fluxes in patients with the same mutation. We will discuss how the model may be used as a starting point to investigate the differences in clinical symptoms between individual patients.

Results

Model construction and characterization

As a starting point for model extension we first considered the previously published human version of the mFAO model [22]. When we simulated MCAD deficiency in this model, no difference in mFAO flux was observed between the MCAD knockout (KO) and WT model at an increasing concentration of the substrate palmitoyl-CoA (C16-acyl-CoA) (Supplementary figure S1). In the WT model MCAD carried little flux (Supplementary Figure S1). We doubt that this is realistic. It might rather be an artifact of parameter fitting when the rat model was converted into a human version [22]. Therefore, we went back to the original rat model, which was based on primary enzyme kinetic data. Where possible, parameters were replaced by values directly measured on human enzymes. The long-chain acyl-CoA (LCAD) isoenzyme was removed, since it is not expressed in human liver [34]. Next, the model was expanded with the pathways depicted in Figure 1, notably ketogenesis, ETF dehydrogenase, mitochondrial ACOT, cytosolic FFA reactivation by ACS, and microsomal omega-oxidation. Furthermore, the export of acyl-carnitines, FFAs and dicarboxylic acids (DCAs) out of the cell were incorporated. For the ketogenesis pathway, all reactions were included, since they directly involve CoA thioesters, CoASH and NAD^+. For the ETF dehydrogenase-catalyzed reaction, ETF, CoQ and its reduced equivalent ($CoQH_2$) were included. To recycle cytosolic acyl-CoA esters generated by ACS into the mFAO, the kinetics of CPT1 had to be adapted. In previous model versions its only substrate was palmitoyl-CoA, but in reality it also converts

other acyl-CoA esters to acyl-carnitines [35]. The omega-oxidation was represented by a single reaction, for which the kinetics of CYP4A11 [36] were used. A mathematical description of the extended model is given in Supplementary text ST1. Figure 2A shows the net steady-state NADH production flux as a function of the concentration of the substrate cytosolic palmitoyl-CoA. An increasing cytosolic palmitoyl-CoA concentration reflects the fasting condition when triglycerides from the adipose stores are hydrolyzed and secreted into the circulation, thus providing more substrate for the liver mFAO. The NADH production flux showed a saturation curve, in which the maximum flux was reached at approximately 30 µM cytosolic palmitoyl-CoA (Figure 2A). At higher substrate concentrations the free CoASH levels declined, mirroring the increase of the total CoA ester concentration in the matrix (Figure 2B). The total CoA concentration was fixed at a constant value, as in previous model versions [22,37], reflecting that CoA biosynthesis takes place at a slower time scale.

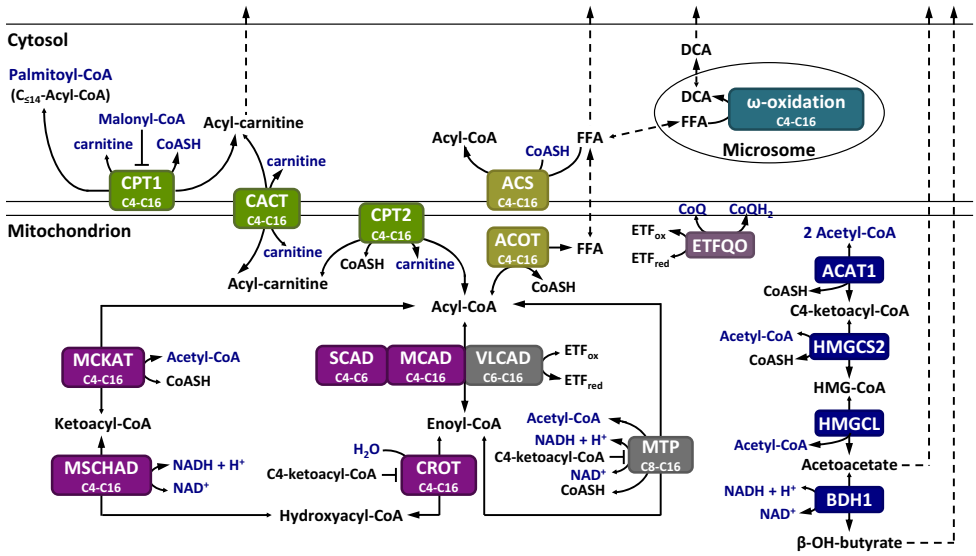

Figure 1. Schematic representation of the extended human model. Metabolites in blue are considered as boundary metabolites with fixed concentrations. The underlying assumption is that their concentrations are determined largely by the surrounding network. The other metabolites are free variables for which ordinary differential equations (ODEs) have been defined (see Supplemental text ST1 for the complete model description). Cytosolic palmitoyl-CoA (given in blue) is the substrate and kept at a fixed concentration, while cytosolic acyl-CoA esters of carbon chain lengths of 14 or lower (indicated by $C_{\leq 14}$, in black) are variable. They are intermediate metabolites derived from the partial oxidation of palmitoyl-CoA and recycling by ACS.

In comparison to **Chapter 2**, we note that the CoASH concentration does not drop to the point where the flux started to decline in the earlier model version. It is possible that this is caused by the addition of processes that regenerate CoASH and reduce the accumulation of CoA esters. The different parameters for the human enzymes may, however, also contribute. We did not investigate this further.

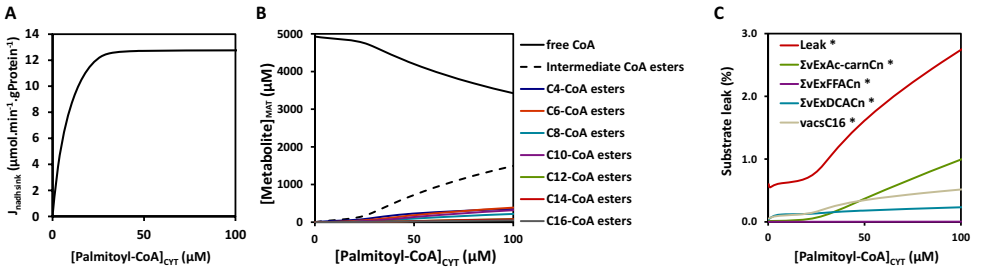

Figure 2. The net NADH production flux in the mitochondrion (i.e production by M/SCHAD and MTP minus consumption by ketogenesis) (denoted in the graph as nadhsink, since at steady state this flux implicity also represents the rate of NADH consumption by oxidative phosphorylation, the sink (**A**); and the mitochondrial CoA ester concentrations, summed over acyl-CoA, enoyl-CoA, hydroxy-enoyl-CoA and ketoacyl-CoA, specified per carbon-chain length (**B**) (cf. Figure 1). Panel **C** depicts 'leak' fluxes of acyl-groups that leave the system via export of acyl-carnitines and FFA or via ω-oxidation, and the C16-acyl-recycling flux via ACS. The fluxes were first calculated in units of NADH that would have been produced if they had been fully oxidized, i.e. a C16-acyl flux would be multiplied by 7, a C14-acyl flux by 6, etc. This allows direct comparison of the fluxes to the net mFAO NADH flux in panel A and to each other (**Supplementary Figure S2**). Subsequently, these fluxes were converted to a percentage of the palmitoyl-CoA consumption flux expressed as NADH production equivalents (100%*flux/(7*vcpt1C16)).

Leakage of acyl-moieties out of the system via export or ω-oxidation was very small (together maximally 2.7 % of the total palmitoyl-CoA consumption flux; (Figure 2C, D). This results in a net NADH production flux similar to the expected NADH production flux if all palmitoyl-CoA would be fully oxidized in the mFAO, i.e. based on 7x the C16-acyl-CoA consumption flux (Supplementary figure S2). Finally, Metabolic Control Analysis (cf. Chapter 2) showed that CPT1 and ETF dehydrogenase (ETFQO) share flux control at 25 μM palmitoyl-CoA_{CYT}, but at at 100 μM palmitoyl-CoA CPT1 does not exert any flux control anymore. As expected, CPT1 has a negative control on CoASH, which was more pronounced at 100 μM palmitoyl-CoA. This is balanced by a positive control exerted by ETFQO (Supplementary table ST1).

Simulating the impact of ACAD deficiencies on the mitochondrial mFAO flux

Next, the impact of a complete inactivation of each of the ACADs was simulated separately, to mimic the corresponding enzyme deficiencies in patients [10,38,39] (Figure 3). A complete inactivation of the enzymes is realistic: both in VLCADD [38] and MCADD [40] residual activities lower than 0.5% have been reported and in SCADD a residual activity lower than 4% has been reported [41]. The VLCAD KO exhibited the lowest NADH production flux, followed by the MCAD KO, while the flux in the SCAD KO model was only marginally lower than that of the WT (Figure 3A). This reflects the general order of disease severity of the human ACAD deficiencies: SCADD is usually asymptomatic[6], MCADD presents only during intercurrent illness or upon another trigger (see above), while VLCADD has the most severe symptoms. Clearly, this model simulates the human diseases better than the previously published human model (Figure 3A). Like the WT (Figure 2B) also the ACAD deficient models showed a decline of CoASH with increasing palmitoyl-CoA concentration (Figure 3B-D). In the VLCAD KO model the decline of CoASH was less than in the WT.

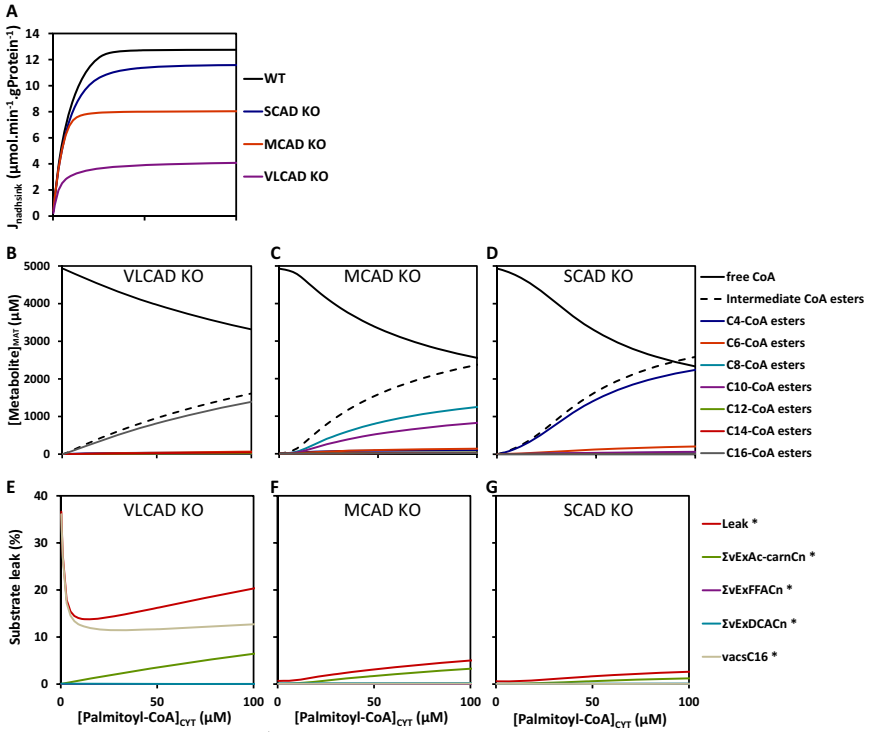

Figure 3. The net NADH production flux in the mFAO (**A**), mitochondrial CoA ester concentrations, summed over acyl-CoA, enoyl-CoA, hydroxy-enoyl-CoA and ketoacyl-CoA, specified per carbon-chain length of WT (healthy) and single-enzyme KO versions of the extended model (**B-D**). Panels **E-G** depict, for each single-enzyme KO model, the 'leak' fluxes of acyl-groups that leave the system via export of acyl-carnitines and FFA or via ω-oxidation, and the C16-acyl-recycling flux via ACS as a percentage of the palmitoyl-CoA consumption flux expressed as NADH production equivalents.

This should be expected, since VLCAD is one of the first enzymes in the pathway and a deficiency prevents accumulation of CoA esters downstream. Accordingly, in the VLCAD KO model only C16-CoA esters accumulated (Figure 3B). In contrast, in the MCAD KO model the decline of CoASH was larger than in the WT model and it was even larger in the SCAD KO model. In these cases, the defect is further downstream, such that substrate enters normally and then starts accumulating. In the MCAD KO model mostly C8 and C10 CoA esters accumulated (Figure 3C), which is consistent with the accumulation of C8 and C10 acyl-carnitines in blood samples from MCADD patients [42–46].

In the SCAD KO model, accumulation of C4-CoA esters was most prominent (Figure 3D), in line with a defect in the metabolism of short-chain acyl-CoA esters and observations in patients. The leak fluxes, *i.e.* the sum of the fluxes of incompletely oxidized palmitoyl-CoA, was very small in the MCAD and SCAD KO models, as it was in the healthy model (cf. Figure 2C-D and Figure 3F-G).In contrast, in the VLCAD KO model the leak was quite a large fraction of the total palmitoyl-CoA consumption flux. The larger fraction of the total leak was, however, recycled through ACS (pink line in Figure 3E). This reflects the general order of disease severity of the human ACAD deficiencies: SCADD is usually asymptomatic[6], MCADD presents only during intercurrent illness or upon another trigger (see above), while

VLCADD has the most severe symptoms. Clearly, this model simulates the human diseases better than the previously published human model (Figure 3A). Like the WT (Figure 2B) also the ACAD deficient models showed a decline of CoASH with increasing palmitoyl-CoA concentration (Figure 3B-D). In the VLCAD KO model the decline of CoASH was less than in the WT. This should be expected, since VLCAD is one of the first enzymes in the pathway and a deficiency prevents accumulation of CoA esters downstream. Accordingly, in the VLCAD KO model only C16-CoA esters accumulated (Figure 3B). In contrast, in the MCAD KO model the decline of CoASH was larger than in the WT model and it was even larger in the SCAD KO model. In these cases, the defect is further downstream, such that substrate enters normally and then starts accumulating. In the MCAD KO model mostly C8 and C10 CoA esters accumulated (Figure 3C), which is consistent with the accumulation of C8 and C10 acyl-carnitines in blood samples from MCADD patients [42–46]. In the SCAD KO model, accumulation of C4-CoA esters was most prominent (Figure 3D), in line with a defect in the metabolism of short-chain acyl-CoA esters and observations in patients. The leak fluxes, *i.e.* the sum of the fluxes of incompletely oxidized palmitoyl-CoA, was very small in the MCAD and SCAD KO models, as it was in the healthy model (cf. Figure 2C-D and Figure 3F-G).In contrast, in the VLCAD KO model the leak was quite a large fraction of the total palmitoyl-CoA consumption flux. The larger fraction of the total leak was, however, recycled through ACS (pink line in Figure 3E).

Impact of individual variations on the mFAO flux

Individual variations in the metabolic pathways that surround the mFAO may affect the mFAO flux and thereby disease presentation. Therefore, a number of variations were tested in the model, with a focus on reduction of the availability of CoASH or NAD^+. We simulated the impact of lower total CoA concentration in the matrix (reflecting a less active CoA biosynthesis or lower concentration of its precursor vitamin B5). We also simulated the impact of lower NAD^+-NADH ratio (reflecting a less active OXPHOS), the effect of a lower cytosolic and mitochondrial L-carnitine concentration (reflecting potentially lower L-carnitine levels in MCADD patients) and a lack of acyl-carnitine export into the blood, as was the case in the published isolated mFAO models [22,47]. Furthermore, we simulated the effect of the absence of ACAT1, the first enzyme of the ketogenesis pathway by setting it's V_{max} to zero (V_{ACAT1}=0) and the impact of knockdown of the thioesterases ACOT by reducing its V_{max} to 1% of its reference value. Finally, we simulated the effect of a knockdown of MCKAT by lowering its V_{max} to 1% of its reference value (Figure 4). Most of the variations that we introduced, had only a minor impact on the net NADH production flux, as can be seen from the relatively small difference between the solid lines and the corresponding dashed lines in Figure 4A-G. This may reflect that the large number of model extensions has made the model relatively robust against these variations.

We did not test whether a human model without these extensions would be more sensitive to reduction of the coenzymes. We observed previously, however, that the rat model without the extensions, was very sensitive to changes in the NAD^+/NADH ratio [26,48]. That ACAT1 had little effect (Figure 4E) may be due to the fact that it catalyzes a reaction that is also catalyzed by MCKAT. MCKAT deficiency had a larger effect than ACAT1 deficiency (cf. Figure 4G and F, respectively).

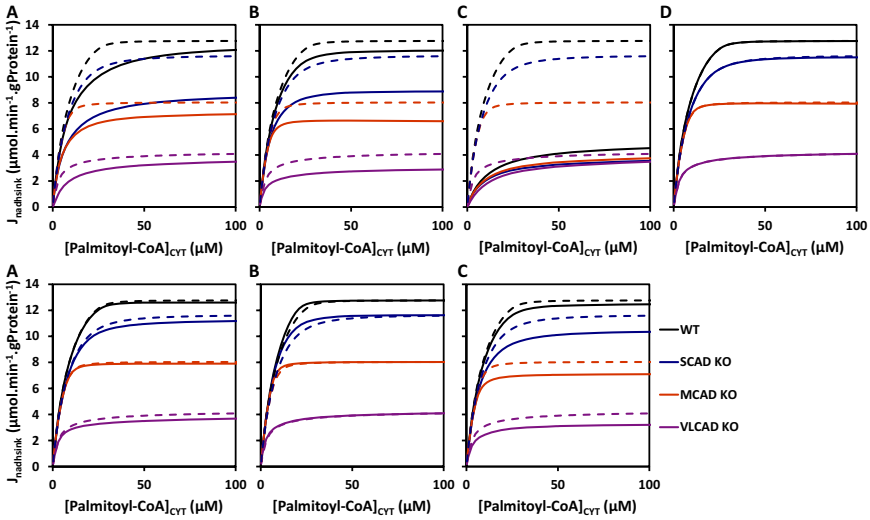

Figure 4. Net NADH production flux (termed nadhsink) of WT and single-enzyme KO versions of the model subjected to additional interventions. The interventions are lower total CoA concentration in the matrix (25% of the reference state) (**A**), lower NAD^+/NADH ratio (25% of the reference state) (**B**), lower cytosolic and mitochondrial L-carnitine concentration (25% of the reference state) (**C**), no acyl-carnitine export into the blood (**D**), no V_{ACAT1} (**E**), lower V_{ACOT} (1% of the reference state) (**F**), lower V_{MCKAT} (25% of the reference state) (**G**). Dashed lines represent the reference state of the WT or the indicated ACAD KO (the same data as in Figure 3), while solid lines represent the indicated variation in these models.

MCKAT, however, converts substrates of a range of carbon-chain lengths varying from C4 till C16. Substrates down to C8 can also be converted by MTP (Figure 1), but MCKAT is an essential enzyme for conversion of C6-ketoacyl-CoA. Of all variations that were imposed, the reduction of cellular L-carnitine levels had the strongest effect on mFAO function (Figure 4C). Carnitine is required for the uptake of acyl-CoA esters through the CPT1-CACT-CPT2 shuttle (Figure 1) and for the export of acyl moieties in the form of acyl-carnitines. Impairment of the export of acyl-carnitines did not affect the mFAO flux (Figure 4D). Therefore, and because CPT1 had substantial control over the flux, we conclude that the reduction of cellular carnitine levels affects the mFAO flux through its role in the shuttle.

Impact of acyl-CoA recycling on the mFAO flux

The thioesterases (ACOTs) have been reported to contribute to the mFAO flux [27–30]. The FFAs that are produced in this reaction can be exported or reactivated by ACS. Therefore, it was investigated whether the FFA reactivation and acyl-CoA recycling has an impact on the mFAO flux. For this, we lowered the V_{max} of ACS to 1% of its reference value. If we only lower the ACS capacity, FFA can still be produced by ACOT and exported, but not reactivated. Lowering ACS however, did not affect the fluxes substantially in the WT or any of the ACAD KOs (Figure 5A). In addition, Metabolic Control Analysis showed that ACS exerted no flux control in the reference model and this was not changed when it was impaired (cf. Supplementary tables ST1 and ST2). The knockdown of ACS enhanced the accumulation of CoA esters and the corresponding reduction of free CoASH in the MCAD KO and SCAD KO models (Figure 5B-E).

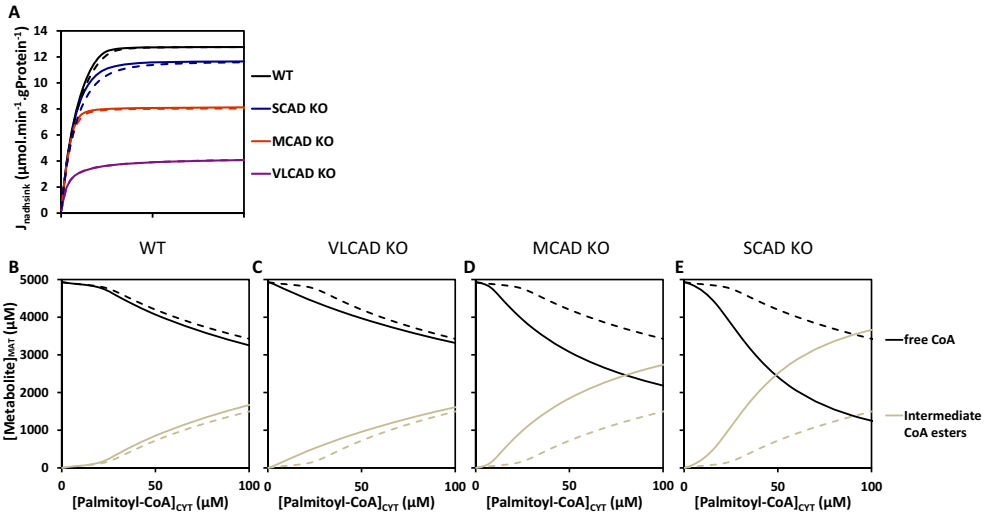

Figure 5. Simulation results of the ACS-knockdown to 1% of its reference value. Reported are the net NADH production flux in the mFAO (A), mitochondrial free CoA and CoA ester concentrations (B-E) In panel A the dashed lines represent the reference state of the WT or the indicated ACAD KO (the same data as in Figure 3), while solid lines represent the ACS knockdown.

Apparently the thioesterase – ACS cycle relieved the sequestration of CoASH. The fluxes of the leakage reaction rates remained low in this model (Supplementary Figure S3). Another way to investigate whether the FFA reactivation and acyl-CoA recycling has an impact on the mFAO flux is by impairing the conversion of the reactivated FFAs (cytosolic C14-C4 acyl-CoA esters) to acyl-carnitines by CPT1. This was done by making CPT1 more C16-specific, *i.e.* by lowering the V_{max} values of CPT1 for the C14-C4 reactions and by lowering its affinity towards C14-C4 acyl-CoA esters (see Supplementary text ST1 for the corresponding kinetic parameters). The latter was achieved by increasing the corresponding K_m values. This modification had little effect on the mFAO flux in the WT, VLCAD KO and SCAD KO (Figure 6A). The mFAO flux of the MCAD KO was substantially reduced however by the impairment of acyl-CoA recycling through CPT1 (Figure 6A). In contrast to the reference model, the C16-specific CPT1 maintained 100% control over the mFAO flux over the whole range of cytosolic palmitoyl-CoA concentrations (Supplementary Table ST3). Surprisingly, the accumulation of mitochondrial CoA esters was completely abolished in the WT and MCAD KO model with a C16-specific CPT1 (Figure 6B-E). Notably, the cytosolic CoA ester concentrations of all the models accumulated to very high levels, since no moiety conservation for cytosolic CoA was imposed (Supplementary table ST4). The fluxes of the leakage reaction rates remained low in this model (Supplementary Figure S4). The MCAD KO model with a C16-specific CPT1 was much more sensitive to additional triggers: when either the total mitochondrial CoA or the total L-carnitine level was reduced by 10%, this led to a strong reduction of the mFAO flux, down to the level of the VLCAD KO model (Figure 6F,G). Considering the severely of VLCADD, is it likely that this is a flux reduction that corresponds to a clinical phenotype.

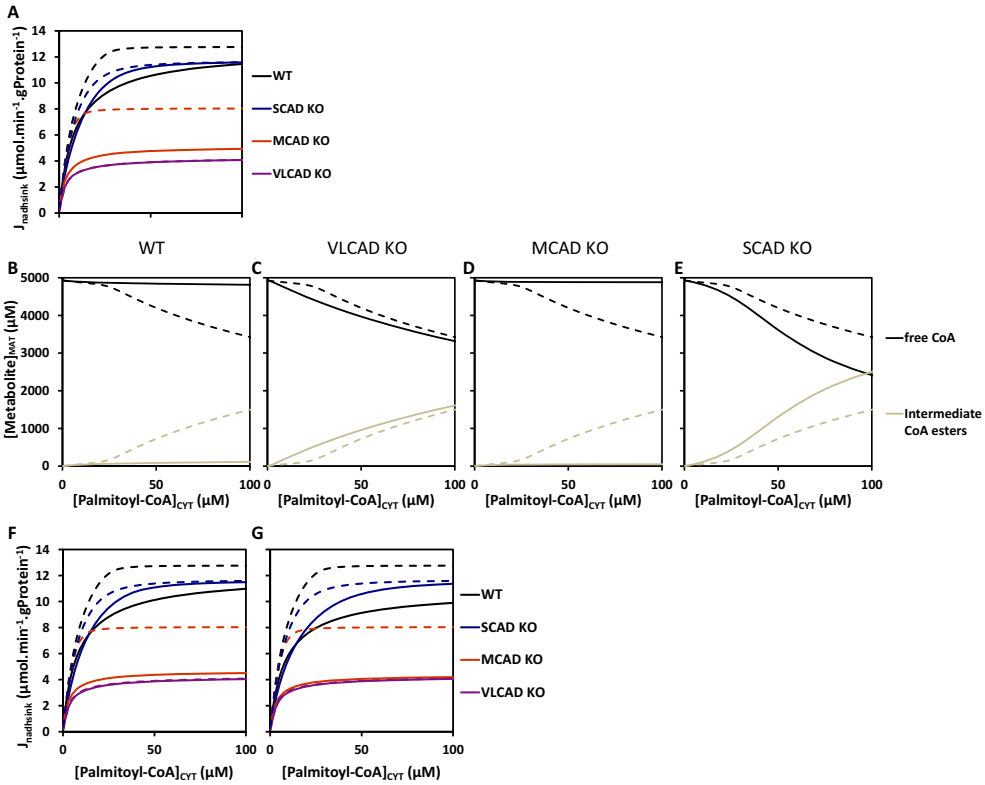

Figure 6. Simulation results of the extended model with a CPT1 with reduced activity and affinity towards C14-C4 acyl-CoA substrates. The parameter values that were changed to obtain this CPT1, are given in the second table in supplementary text ST1. Reported are the total NADH production flux in the mFAO (**A**) and the mitochondrial CoASH and CoA ester concentrations (C16-C4 acyl-CoA esters) (**B-E**). Panels **F-G** display the net NADH production flux (termed nadhsink) of WT and single-enzyme KO versions of the model subjected to additional interventions. The interventions are lower total CoA concentration in the matrix (90% of the reference state) (**F**) and lower cytosolic and mitochondrial L-carnitine concentration (90% of the reference state) (**G**). Dashed lines represent the reference state of the WT or the indicated ACAD KO (the same data as in **Figure 3**), while solid lines represent the indicated variation in these models.

Discussion

The mFAO pathway is intricately connected to several pathways of energy metabolism. These pathways may play a particularly crucial role in the function of mFAO in the liver during fasting or conditions of high energy demand. In this study, we generated for the first time, a dynamic computational model of mFAO in human liver with extensions into the major pathways that affect the acyl-CoA and CoASH concentrations. Such a model is an important tool to get a more realistic impression of the mechanisms leading to robustness and vulnerability in mFAOD. Particularly, in MCADD, disease severity cannot be predicted even within the same mutation [7–15]. Our aim was to investigate whether the different disease presentations of patients could theoretically be caused by individual variations in the surrounding network. A computational model does not prove that such variations

actually play a role in patients, but they give insight in which variations, if they occurred, could have the strongest impact *in vivo*. For this we characterized the model and introduced perturbations that were expected to be relevant in MCADD.

Metabolic control analysis showed that CPT1 shared control with ETF dehydrogenase in the model. CPT1 lost flux control at high palmitoyl-CoA concentrations. This is different from the previously published rat model (without extensions) in which CPT1 got a negative flux control coefficient at high substrate concentrations [48]. The relative fluxes of the ACAD KO models were in agreement with general disease severity of ACADD in humans (reference WT and KO models). In addition, the ACAD KO models showed acyl-CoA profiles in the mitochondrial matrix that are similar to the corresponding acyl-carnitine profiles in patients. Based on expected importance of several enzymes and metabolites in MCADD, we determined the effect of changing select related parameters on the flux of the WT and ACAD KO models. Most of these parameters had a small effect on the fluxes in the ACAD KO models. Lowering L-carnitine, however, had an indiscriminately strong effect on all the ACAD KO models.

We next investigated the importance of FFA recycling in this model, through the futile cycle of mitochondrial acyl-CoA hydrolysis, export into the cytosol, reactivation by ACS and uptake back into the mitochondria. However, impaired ACS activity did not affect the mFAO flux in any of the ACAD KO models. Potentially, the impact of this cycle was minimal due to the relatively small flux through ACS. Flux analysis experiments *in vitro* could provide more information on the ratio of ACS versus mFAO flux in cells, in order to be able to simulate the role of the ACS-mediated reactivation system more realistically.

Finally, we investigated the effect of changing CPT1 kinetics, to study its role in the recycling of FFA via ACS. Interestingly, particularly the MCAD KO version of the model was sensitive to alterations of the parameters involved in recycling of C4-C14 acyl-CoA esters. In addition, *in silico* perturbations that had no phenotype in the reference MCAD KO model, resulted in a strong decrease of the mFAO flux in the MCAD KO model with the altered CPT1 kinetics. We currently have no evidence for the existence of mutations in CPT1 that have such effects on CPT1 kinetics. Given that CPT1 is known to have a high control over mFAO flux under specific conditions [49,50] and that our model predicts such a strong effect of a CPT1 kinetics in the MCAD KO model, it may be interesting to investigate whether CPT1 might play a role in the vulnerability of some symptomatic MCADD individuals. To investigate this, it would be relevant to investigate mutations in the CPT1 gene in the general population and in symptomatic versus asymptomatic MCAD deficient children. Moreover, exome sequencing of symptomatic versus asymptomatic MCAD children may yield candidate genes that can be tested functionally in the computational model. This should allow us to select the most promising candidates for further in vitro testing.

In this initial study we have not yet considered certain factors, reactions or pathways. For instance, we did not allow for conserved moieties of carnitine in the matrix and cytosol and total CoA (free and acylated CoA) in the cytosol, as these could limit the acyl-carnitine and CoA ester concentrations in the model. We do not think that this will invalidate the conclusions of this study. We have also not reported which parameters may have contributed to an absence in flux decline as was observed in the WT rat model of the isolated mFAO, but not in in the WT version of the fitted mouse model of the isolated mFAO. We note that in [22], where a mouse and human model of isolate mFAO was presented this

difference was also not investigated, potentially to focus on a the role of enzyme promiscuity on the flux and metabolite profiles. Here we focused on the effect of genetic and environmental modifiers on mFAO flux in MCADD and note that it was not necessary for the models to show flux decline in order to answer our research question. We have therefore deemed it not necessary to report which parameters or combination of parameters affect the presence or absence of flux decline in this study. We also make the preliminary conclusion that flux decline is not a necessary or persistent phenomenon even in isolated mFAO models. We have also not included mitochondrial medium-chain FFA reactivation, cytosolic acyl-CoA hydrolysis and peroxisomal fatty-acid beta oxidation of medium-chain DCAs. However, in this initial study we have decided to focus on the characterization of a human model containing the most important reactions and pathways for which substantial evidence has been given for their role in mFAO flux. This preliminary model is therefore also smaller and easier to characterize. As indicated, the absence of elements in the model does not necessarily invalidate the conclusions in this study, but instead offer new avenues for identifying modifiers that could affect symptomatology in MCADD in specific and mFAOD in general.

Materials and Methods

Model construction and simulation

The model was built and the simulations and calculations were done in Wolfram Mathematica (Wolfram Research, Inc., Champaign, IL, USA), version 11.3.0.0. A full description of the model equations is given in Supplementary Text ST1. All the steady-state data were generated from the steady-state initial condition at a cytosolic palmitoyl-CoA concentration ($[\text{palmitoyl-CoA}]_{CYT}$) of 0.1 μM, which is exactly as done in our previous paper [21]. The Mathematica functions NDSolve and FindRoot were used to generate the simulation results, as done in [37,51]. The model has multiple independent fluxes. Here, we focused on the net mitochondrial NADH production flux, which equals the implied external NADH reoxidation rate that would result in the maintenance of a constant NAD^+-NADH ratio. Therefore, we used the term nadhsink to depict the net NADH production fluxes in y-axes of the graphs in this study ($J_{nadhsink}$), as was done in our previous papers [26,51]. We did not check if the steady state was unique.

Flux control analysis

Flux control coefficients were approximated according to:

$$C_{enzyme}^{J} = \frac{dlnJ/dp}{\partial lnv/\partial p} \approx \frac{\Delta J}{\Delta V_{max,enzyme}} \cdot \frac{V_{max,enzyme}}{J} \quad (1)$$

where p denotes a parameter that only affects the rate of the enzyme that is analyzed. V_{max} was used since the rates of all reactions were proportional to this parameter. For the finite change denoted by Δ a percentage below 3% taken, and the result was accepted if the sum of all flux control coefficients in the model was equal to 1 [52,53].

References

1. Houten SM, Wanders RJA. A general introduction to the biochemistry of mitochondrial fatty acid β-oxidation. J Inherit Metab Dis. 2010;33(5):469–77.
2. Eaton S, Bartlett K, Pourfarzam M. Mammalian mitochondrial beta-oxidation. Biochem J. 1996;320:345–57.
3. Houten SM, Violante S, Ventura F V., Wanders RJA. The Biochemistry and Physiology of

Mitochondrial Fatty Acid β-Oxidation and Its Genetic Disorders. Annu Rev Physiol. 2016;78(1):23–44.
4. van Eunen K, Volker-Touw CML, Gerding A, Bleeker A, Wolters JC, van Rijt WJ, Martines ACMF, Niezen-Koning KE, Heiner RM, Permentier H, Groen AK, Reijngoud DJ, Derks TGJ, Bakker BM. Living on the edge: Substrate competition explains loss of robustness in mitochondrial fatty-acid oxidation disorders. BMC Biol. 2016;14(1):1–15.
5. Rinaldo P, Matern D, Bennett MJ. Fatty Acid oxidation Disorders. Annu Rev Physiol. 2002;64(1):477–502.
6. Houten SM, Violante S, Ventura F V, Wanders RJA. The Biochemistry and Physiology of Mitochondrial Fatty Acid β-Oxidation and Its Genetic Disorders. Annu Rev Physiol. 2015;78:23–44.
7. Derks TGJ, Reijngoud DJ, Waterham HR, Gerver WJM, van den Berg MP, Sauer PJJ, Smit GPA. The natural history of medium-chain acyl CoA dehydrogenase deficiency in the Netherlands: Clinical presentation and outcome. J Pediatr. 2006;148(5).
8. Derks TGJ, Boer TS, Assen A, Bos T, Ruiter J, Waterham HR, Niezen-Koning KE, Wanders RJA, Rondeel JMM, Loeber JG, Te Kate LP, Smit GPA, Reijngoud DJ. Neonatal screening for medium-chain acyl-CoA dehydrogenase (MCAD) deficiency in The Netherlands: The importance of enzyme analysis to ascertain true MCAD deficiency. J Inherit Metab Dis. 2008;31(1):88–96.
9. Touw CML, Smit GPA, Niezen-Koning KE, Bosgraaf-de Boer C, Gerding A, Reijngoud D-J, Derks TGJ. In vitro and in vivo consequences of variant medium-chain acyl-CoA dehydrogenase genotypes. Orphanet J Rare Dis. 2013;8(1):43.
10. Touw CML, Smit GPA, de Vries M, de Klerk JBC, Bosch AM, Visser G, Mulder MF, Rubio-Gozalbo ME, Elvers B, Niezen-Koning KE, Wanders RJA, Waterham HR, Reijngoud D-J, Derks TGJ. Risk stratification by residual enzyme activity after newborn screening for medium-chain acyl-CoA dehyrogenase deficiency: data from a cohort study. Orphanet J Rare Dis. 2012;7:30.
11. Spiekerkoetter U, Bastin J, Gillingham M, Morris A, Wijburg F, Wilcken B. Current issues regarding treatment of mitochondrial fatty acid oxidation disorders. J Inherit Metab Dis. 2010;33(5):555–61.
12. Fromenty B, Mansouri a, Bonnefont JP, Courtois F, Munnich a, Rabier D, PessayreD. Most cases of medium-chain acyl-CoA dehydrogenase deficiency escape detection in France. Hum Genet. 1996;97(3):367–8.
13. Kelly DP, Whelan AJ, Ogden ML, Alpers R, Zhang ZF, Bellus G, Gregersen N, Dorland L, Strauss AW. Molecular characterization of inherited medium-chain acyl-CoA dehydrogenase deficiency. Proc Natl Acad Sci. 1990;87(23):9236–40.
14. Duran M, Hofkamp M, Rhead WJ, Saudubray J-M, Wadman SK. Sudden Child Death and `Healthy' Affected Family Members With Medium-Chain Acyl-Coenzyme A Dehydrogenase Deficiency. Pediatrics. 1986;78(6):1052–7.
15. Schatz U a., Ensenauer R. The clinical manifestation of MCAD deficiency: Challenges towards adulthood in the screened population. J Inherit Metab Dis. 2010;33(5):513–20.
16. Derks TGJ, Van Spronsen FJ, Rake JP, Van Der Hilst CS, Span MM, Smit GPA. Safe and unsafe duration of fasting for children with MCAD deficiency. Eur J Pediatr. 2007;166(1):5–11.
17. Walter JH. Tolerance to fast: Rational and practical evaluation in children with hypoketonaemia. J Inherit Metab Dis. 2009;32(2):214–7.
18. Bennett MJ. Pathophysiology of fatty acid oxidation disorders. J Inherit Metab Dis. 2010;33(5):533–7.
19. Vishwanath VA. Fatty acid beta-oxidation disorders: A brief review. Ann Neurosci. 2016;23(1):51–5.
20. Volker-touw CML. MCAD deficiency To be , or not to be at risk. 2014.
21. Martines A-CMF, van Eunen K, Reijngoud D-J, Bakker BM. The promiscuous enzyme medium-

chain 3-keto-acyl-CoA thiolase triggers a vicious cycle in fatty-acid beta-oxidation. PLOS Comput Biol. 2017;13(4):1–22.

22. van Eunen K, Volker-Touw CML, Gerding A, Bleeker A, Wolters JC, van Rijt WJ, Martines ACMF, Niezen-Koning KE, Heiner RM, Permentier H, Groen AK, Reijngoud DJ, Derks TGJ, Bakker BM. Living on the edge: Substrate competition explains loss of robustness in mitochondrial fatty-acid oxidation disorders. BMC Biol. 2016;14(1):1–15.
23. Yamaoka K, Kanayama M, Tajiri K, Yamane M, Marumo F, Sato C. Clinical significance of arterial ketone body ratio in chronic liver disease. Digestion. 2003;59(4):360–3.
24. Ukikusa M, Ozawa K, Shimahara Y, Asano M, Nakatani T, Tobe T. Changes in blood ketone body ratio: their significance after major hepatic resection. Arch Surg. 1981 Jun;116(6):781–5.
25. Lim SC, Tajika M, Shimura M, Carey KT, Stroud DA, Murayama K, Ohtake A, Mckenzie M. Loss of the Mitochondrial Fatty Acid β-Oxidation Protein Medium-Chain Acyl-Coenzyme A Dehydrogenase Disrupts Oxidative Phosphorylation Protein Complex Stability and Function. Sci Rep. 2018;(December 2017):1–17.
26. van Eunen K, Simons SMJ, Gerding A, Bleeker A, den Besten G, Touw CML, Houten SM, Groen BK, Krab K, Reijngoud DJ, Bakker BM. Biochemical Competition Makes Fatty-Acid β-Oxidation Vulnerable to Substrate Overload. PLoS Comput Biol. 2013;9(8):2–9.
27. Moffat C, Bhatia L, Nguyen T, Lynch P, Wang M, Wang D, Ilkayeva OR, Han X, Hirschey MD, Claypool SM, Seifert EL. Acyl-CoA thioesterase-2 facilitates mitochondrial fatty acid oxidation in the liver. J Lipid Res. 2014;55(12):2458–70.
28. Ellis JM, Bowman CE, Wolfgang MJ. Metabolic and Tissue-Specific Regulation of Acyl-CoA Metabolism. PLoS One. 2015;10(3).
29. Tillander V, Alexson SEH, Cohen DE. Deactivating Fatty Acids: Acyl-CoA Thioesterase-Mediated Control of Lipid Metabolism. Trends Endocrinol Metab. 2017;28(7):473–84.
30. Hunt MC, Alexson SE. The role Acyl-CoA thioesterases play in mediating intracellular lipid metabolism. Prog Lipid Res. 2002;41(2):99–130.
31. Wanders RJA, Komen J, Kemp S. Fatty acid omega-oxidation as a rescue pathway for fatty acid oxidation disorders in humans. FEBS J. 2011;278(2):182–94.
32. Mitchell GA, Gauthier N, Lesimple A, Wang SP, Mamer O, Qureshi I. Hereditary and acquired diseases of acyl-coenzyme A metabolism. Mol Genet Metab. 2008;94(1):4–15.
33. Yang H, Zhao C, Wang Y, Wang SP, Mitchell GA. Hereditary diseases of coenzyme A thioester metabolism. Biochem Soc Trans. 2019 Feb 28;47(1):149–55.
34. Wolters JC, Ciapaite J, Van Eunen K, Niezen-Koning KE, Matton A, Porte RJ, Horvatovich P, Bakker BM, Bischoff R, Permentier HP. Translational Targeted Proteomics Profiling of Mitochondrial Energy Metabolic Pathways in Mouse and Human Samples. J Proteome Res. 2016;15(9):3204–13.
35. Finocchiaro G, Colombo I, DiDonato S. Purification, characterization and partial amino acid sequences of carnitine palmitoyl-transferase from human liver. FEBS Lett. 1990;274(1–2):163–6.
36. Gregersen N, Mortensen PB, Kølvraa S. On the biologic origin of C6-C10-dicarboxylic and C6-C10-omega-1- hydroxy monocarboxylic acids in human and rat with acyl-CoA dehydrogenation deficiencies: in vitro studies on the omega- and omega-1-oxidation of medium-chain (C6-C12) fatty acids in human . PediatrRes. 1983;17(10):828–34.
37. van Eunen K, Simons SMJ, Gerding A, Bleeker A, den Besten G, Touw CML, Houten SM, Groen BK, Krab K, Reijngoud DJ, Bakker BM. Biochemical Competition Makes Fatty-Acid Beta-Oxidation Vulnerable to Substrate Overload. PLoS Comput Biol. 2013;9(8):2–9.
38. ter Veld F, Mueller M, Kramer S, Haussmann U, Herebian D, Mayatepek E, Laryea MD, Primassin S, Spiekerkoetter U. A novel tandem mass spectrometry method for rapid confirmation of medium- and very long-chain acyl-CoA dehydrogenase deficiency in

newborns. PLoS One. 2009;4(7).
39. Bok LA, Vreken P, Wijburg FA, Wanders RJA, Gregersen N, Corydon MJ, Waterham HR, Duran M. Short-Chain Acyl-CoA Dehydrogenase Deficiency: Studies in a Large Family Adding to the Complexity of the Disorder. Pediatrics. 2003;112(5):1152–5.
40. Touw CML, Smit GPA, de Vries M, de Klerk JBC, Bosch AM, Visser G, Mulder MF, Rubio-Gozalbo ME, Elvers B, Niezen-Koning KE, Wanders RJA, Waterham HR, Reijngoud D-J, Derks TGJ. Risk stratification by residual enzyme activity after newborn screening for medium-chain acyl-CoA dehyrogenase deficiency: data from a cohort study. Orphanet J Rare Dis. 2012 May 25;7(1):30.
41. Bok LA, Vreken P, Wijburg FA, Wanders RJA, Gregersen N, Corydon MJ, Waterham HR, Duran M. Short-chain Acyl-CoA dehydrogenase deficiency: studies in a large family adding to the complexity of the disorder. Pediatrics. 2003 Nov;112(5):1152–5.
42. Vianey-Liaud C, Divry P, Gregersen N, Mathieu M. The inborn errors of mitochondrial fatty acid oxidation. J Inher Metab Dis. 1987;10:159–200.
43. Touma E, Charpentier C. Medium chain acyl-CoA dehydrogenase deficiency. Arch Dis Child. 1992;67:142–5.
44. Bentler K, Zhai S, Elsbecker SA, Arnold GL, Burton BK, Vockley J, Cameron CA, Hiner SJ, Edick MJ, Berry SA, Thomas J, Dodge M, Singh R, Lakshman S, Coakley K, Stembridge A, Russi AS, Phillips E, Burton B, Edano C, Shrestha S, Hoganson G, Dwyer L, Hainline B, Romie S, Hainline S, Asamoah A, Goodin K, Rajakaruna C, Jackson K, Hamosh A, Vernon H, Smith N, Ahmad A, Lipinski S, Feldman G, Berry S, Elsbecker S, Bentler K, Font-Montgomery E, Peck D, Pena LDM, Koeberl DD, Jiang Y hui, Kishnani PS, Rizzo W, Dawson M, Ambrose N, Levy P, Kronn D, Fong C to, D'Aco K, Hart T, Erbe R, Samons M, Leslie N, Powers R, Bartholomew D, Goff M, vanCalcar S, Hansen J, Arnold G, Vockley J, Walsh-Vockley C, Rhead W, Dimmock D, Engelking P, Bird C, Swan A, Schwoerer JS, Henry S, Narumanchi TC, Hummel M, Wilkins J, Davis-Keppen L, Stein Q, Loman R, Cameron C, Edick MJ, Hiner SJ, Justice K, Zhai S. 221 newborn-screened neonates with medium-chain acyl-coenzyme A dehydrogenase deficiency: Findings from the Inborn Errors of Metabolism Collaborative. Mol Genet Metab. 2016;119(1–2):75–82.
45. Walter JH. L-Carnitine in inborn errors of metabolism: What is the evidence? J Inherit Metab Dis. 2003;26(2–3):181–8.
46. Roe CR. Inherited disorders of mitochondrial fatty acid oxidation: A new responsibility for the neonatologist. Semin Neonatol. 2002;7(1):37–47.
47. van Eunen K, Simons SMJ, Gerding A, Bleeker A, den Besten G, Touw CML, Houten SM, Groen BK, Krab K, Reijngoud DJ, Bakker BM. Biochemical Competition Makes Fatty-Acid β-Oxidation Vulnerable to Substrate Overload. PLoS Comput Biol. 2013;9(8):2–9.
48. Martines ACMF, van Eunen K, Reijngoud DJ, Bakker BM. The promiscuous enzyme medium-chain 3-keto-acyl-CoA thiolase triggers a vicious cycle in fatty-acid beta-oxidation. PLoS Comput Biol. 2017;13(4):1–22.
49. Eaton S. Control of mitochondrial b -oxidation flux. 2002;41:197–239.
50. Spurway TD, Sherratt HS a, Pogson CI, Agius L. B-Oxidation in Rat Hepatocyte Cultures. Biochem J. 1997;323:119–22.
51. van Eunen K, Volker-Touw CML, Gerding A, Bleeker A, Wolters JC, van Rijt WJ, Martines A-CMF, Niezen-Koning KE, Heiner RM, Permentier H, Groen AK, Reijngoud D-J, Derks TGJ, Bakker BM. Living on the edge: substrate competition explains loss of robustness in mitochondrial fatty-acid oxidation disorders. BMC Biol. 2016;14(1):107.
52. Hofmeyr JS. Metabolic control analysis in a nutshell. In: Proceedings of the 2nd International conference on systems biology. 2001. p. 291–300.
53. Fell DA. Metabolic control analysis: a survey of its theoretical and experimental development. Biochem J. 1992;286 (Pt 2:313–30.

Supplementary text ST1: Model description

The starting point for the model described here was that of beta-oxidation in rat liver mitochondria[1]. This model has been adapted to represent human liver by removing the LCAD reaction, since this enzyme is hardly expressed in human liver [2]. Moreover, where available, parameters for human enzymes have been used. In addition, the original model has undergone a comprehensive extension, with a focus on the reactions around coenzyme A and the acyl-CoA esters. A visual representation of the reactions included in the new model is given in Figure 1. Whenever parameters were used from the original model, the reference to the corresponding paper [1] is given rather than to the underlying biochemical literature. When other references are given, this indicates that it concerns an extension or an adaptation to the human situation. Fixed boundary metabolites in the original model were kept fixed in this extended model. Many of the variable metabolites depend on the reactions that were added in the extension, hence the Ordinary Differential Equations governing them have changed as described below. In addition, a couple of new differential equations have been introduced for variable metabolites that were newly incorporated. the microsome was incorporated to contain the omega oxidation. The microsome was include as it has its own local concentration of NADPH.

Ordinary differential equations (ODEs)

The ODEs in the model are given below. Cytosolic, mitochondrial matrix and microsome localizations are denoted as CYT, MAT and MICR, respectively. Reaction rates are denoted with a small v and cytosolic, mitochondrial matrix and microsome volumes are denoted with VCYT, VMAT and VMICR, respectively. The forward direction is, for mFAO, the direction of oxidation and for ketogenesis, the direction of ketone body production (which is why therefore for ACAT1, the forward direction is, in contrast to MCKAT, not thiolysis but condensation). The forward direction for each reaction is also given by the direction of the large arrow in Figure 1. As most enzymes catalyze reactions from substrates of more than one chain length, the abbreviation for the rate of a reaction catalyzed by an enzyme, finishes with C and the number of carbons in the acyl-chain of the substrate of the reaction in question. For example, vcpt1C16 represents the rate of the conversion of C16-acyl-CoA (i.e. palmitoyl-CoA) to C16-acyl-carnitine by CPT1.

ODE's from metabolites that were already in the rat model.

Rates that are different compared to the rat model have been indicated in bold.

$$\mathrm{C16AcylCarCYT}'[t] == \frac{-\mathrm{vcactC16}+\mathrm{vcpt1C16}-\mathrm{vExAccC16}}{\mathrm{VCYT}} \quad (1)$$

$$\mathrm{C16AcylCarMAT}'[t] == \frac{\mathrm{vcactC16}-\mathrm{vcpt2C16}}{\mathrm{VMAT}} \quad (2)$$

$$\mathrm{C16AcylCoAMAT}'[t] == \frac{-\mathbf{vacotC16}+\mathrm{vcpt2C16}-\mathbf{vmcadC16}-\mathrm{vvlcadC16}}{\mathrm{VMAT}} \quad (3)$$

$$\mathrm{C16EnoylCoAMAT}'[t] == \frac{-\mathrm{vcrotC16}+\mathrm{v}\mathbf{mcadC16}-\mathrm{vmtpC16}+\mathrm{vvlcadC16}}{\mathrm{VMAT}} \quad (4)$$

$$\mathrm{C16HydroxyacylCoAMAT}'[t] == \frac{\mathrm{vcrotC16}-\mathrm{vmschadC16}}{\mathrm{VMAT}} \quad (5)$$

$$\text{C16KetoacylCoAMAT}'[t] == \frac{-\text{vmckatC16}+\text{vmschadC16}}{\text{VMAT}} \quad (6)$$

$$\text{C14AcylCarCYT}'[t] == \frac{-\text{vcactC14}+\mathbf{vcpt1C14}-\text{vExAccC14}}{\text{VCYT}} \quad (7)$$

$$\text{C14AcylCarMAT}'[t] == \frac{\text{vcactC14}-\text{vcpt2C14}}{\text{VMAT}} \quad (8)$$

$$\text{C14AcylCoAMAT}'[t] == \frac{-\mathbf{vacotC14}+\text{vcpt2C14}-\mathbf{vmcadC14}+\text{vmckatC16}+\text{vmtpC16}-\text{vvlcadC14}}{\text{VMAT}} \quad (9)$$

$$\text{C14EnoylCoAMAT}'[t] == \frac{-\text{vcrotC14}+\mathbf{vmcadC14}-\text{vmtpC14}+\text{vvlcadC14}}{\text{VMAT}} \quad (10)$$

$$\text{C14HydroxyacylCoAMAT}'[t] == \frac{\text{vcrotC14}-\text{vmschadC14}}{\text{VMAT}} \quad (11)$$

$$\text{C14KetoacylCoAMAT}'[t] == \frac{-\text{vmckatC14}+\text{vmschadC14}}{\text{VMAT}} \quad (12)$$

$$\text{C12AcylCarCYT}'[t] == \frac{-\text{vcactC12}+\mathbf{vcpt1C12}-\text{vExAccC12}}{\text{VCYT}} \quad (13)$$

$$\text{C12AcylCarMAT}'[t] == \frac{\text{vcactC12}-\mathbf{vcpt2C12}}{\text{VMAT}} \quad (14)$$

$$\text{C12AcylCoAMAT}'[t] == \frac{-\mathbf{vacotC12}+\text{vcpt2C12}-\text{vmcadC12}+\text{vmckatC14}+\text{vmtpC14}-\text{vvlcadC12}}{\text{VMAT}} \quad (15)$$

$$\text{C12EnoylCoAMAT}'[t] == \frac{-\text{vcrotC12}+\text{vmcadC12}-\text{vmtpC12}+\text{vvlcadC12}}{\text{VMAT}} \quad (16)$$

$$\text{C12HydroxyacylCoAMAT}'[t] == \frac{\text{vcrotC12}-\text{vmschadC12}}{\text{VMAT}} \quad (17)$$

$$\text{C12KetoacylCoAMAT}'[t] == \frac{-\text{vmckatC12}+\text{vmschadC12}}{\text{VMAT}} \quad (18)$$

$$\text{C10AcylCarCYT}'[t] == \frac{-\text{vcactC10}+\text{vcpt1C10}-\text{vExAccC10}}{\text{VCYT}} \quad (19)$$

$$\text{C10AcylCarMAT}'[t] == \frac{\text{vcactC10}-\mathbf{vcpt2C10}}{\text{VMAT}} \quad (20)$$

$$\text{C10AcylCoAMAT}'[t] == \frac{-\mathbf{vacotC10}+\text{vcpt2C10}-\text{vmcadC10}+\text{vmckatC12}+\text{vmtpC12}-\mathbf{vvlcadC10}}{\text{VMAT}} \quad (21)$$

$$\text{C10EnoylCoAMAT}'[t] == \frac{-\text{vcrotC10}+\text{vmcadC10}-\text{vmtpC10}+\mathbf{vvlcadC10}}{\text{VMAT}} \quad (22)$$

$$\text{C10HydroxyacylCoAMAT}'[t] == \frac{\text{vcrotC10}-\text{vmschadC10}}{\text{VMAT}} \quad (23)$$

$$\text{C10KetoacylCoAMAT}'[t] == \frac{-\text{vmckatC10}+\text{vmschadC10}}{\text{VMAT}} \quad (24$$

$$\text{C8AcylCarCYT}'[t] == \frac{-\text{vcactC8}+\mathbf{vcpt1C8}-\text{vExAccC8}}{\text{VCYT}} \quad (25)$$

$$\text{C8AcylCarMAT}'[t] == \frac{\text{vcactC8}-\mathbf{vcpt2C8}}{\text{VMAT}} \quad (26)$$

$$\text{C8AcylCoAMAT}'[t] == \frac{-\mathbf{vacotC8}+\text{vcpt2C8}-\text{vmcadC8}+\text{vmckatC10}+\text{vmtpC10}-\mathbf{vvlcadC8}}{\text{VMAT}} \quad (27)$$

$$\text{C8EnoylCoAMAT}'[t] == \frac{-\text{vcrotC8}+\text{vmcadC8}-\text{vmtpC8}+\mathbf{vvlcadC8}}{\text{VMAT}} \quad (28)$$

$$\text{C8HydroxyacylCoAMAT}'[t] == \frac{\text{vcrotC8} - \text{vmschadC8}}{\text{VMAT}} \quad (29)$$

$$\text{C8KetoacylCoAMAT}'[t] == \frac{-\text{vmckatC8} + \text{vmschadC8}}{\text{VMAT}} \quad (30)$$

$$\text{C6AcylCarCYT}'[t] == \frac{-\text{vcactC6} + \mathbf{vcpt1C6} - \text{vExAccC6}}{\text{VCYT}} \quad (31)$$

$$\text{C6AcylCarMAT}'[t] == \frac{\text{vcactC6} - \text{vcpt2C6}}{\text{VMAT}} \quad (32)$$

$$\text{C6AcylCoAMAT}'[t] == \frac{-\mathbf{vacotC6} + \text{vcpt2C6} - \text{vmcadC6} + \text{vmckatC8} + \text{vmtpC8} - \text{vscadC6} - \mathbf{vvlcadC6}}{\text{VMAT}} \quad (33)$$

$$\text{C6EnoylCoAMAT}'[t] == \frac{-\text{vcrotC6} + \text{vmcadC6} + \text{vscadC6} + \mathbf{vvlcadC6}}{\text{VMAT}} \quad (34))$$

$$\text{C6HydroxyacylCoAMAT}'[t] == \frac{\text{vcrotC6} - \text{vmschadC6}}{\text{VMAT}} \quad (35)$$

$$\text{C6KetoacylCoAMAT}'[t] == \frac{-\text{vmckatC6} + \text{vmschadC6}}{\text{VMAT}} \quad (36)$$

$$\text{C4AcylCarCYT}'[t] == \frac{-\text{vcactC4} + \text{vcpt1C4} - \text{vExAccC4}}{\text{VCYT}} \quad (37)$$

$$\text{C4AcylCarMAT}'[t] == \frac{\text{vcactC4} - \text{vcpt2C4}}{\text{VMAT}} \quad (38)$$

$$\text{C4AcylCoAMAT}'[t] == \frac{-\mathbf{vacotC4} + \text{vcpt2C4} - \text{vmcadC4} + \text{vmckatC6} - \text{vscadC4}}{\text{VMAT}} \quad (39)$$

$$\text{C4EnoylCoAMAT}'[t] == \frac{-\text{vcrotC4} + \text{vmcadC4} + \text{vscadC4}}{\text{VMAT}} \quad (40)$$

$$\text{C4HydroxyacylCoAMAT}'[t] == \frac{\text{vcrotC4} - \text{vmschadC4}}{\text{VMAT}} \quad (41$$

$$\text{C4AcetoacylCoAMAT}'[t] == \frac{\text{vacat1} - \text{vhmgcs2} - \text{vmckatC4} + \text{vmschadC4}}{\text{VMAT}} \quad (42)$$

ODEs from newly introduced metabolites.

$$\text{ETFhqMAT}'[t] == \frac{\begin{matrix}\text{vvlcadC16} + \text{vvlcadC14} + \text{vvlcadC12} + \text{vvlcadC10} + \text{vvlcadC8} + \text{vvlcadC6} + \text{vmcadC16} \\ +\text{vmcadC14} + \text{vmcadC12} + \text{vmcadC10} + \text{vmcadC8} + \text{vmcadC6} + \text{vmcadC4} + \text{vscadC6} + \text{vscadC4} - \text{vetfqo}\end{matrix}}{\text{VMAT}}$$

(43

$$\text{C16FFAMAT}'[t] == \frac{\text{vacotC16} - \text{vmcFFAC16}}{\text{VMAT}} \quad (44)$$

$$\text{C14FFAMAT}'[t] == \frac{\text{vacotC14} - \text{vmcFFAC14}}{\text{VMAT}} \quad (45)$$

$$\text{C12FFAMAT}'[t] == \frac{\text{vacotC12} - \text{vmcFFAC12}}{\text{VMAT}} \quad (46)$$

$$\text{C10FFAMAT}'[t] == \frac{\text{vacotC10} - \text{vmcFFAC10}}{\text{VMAT}} \quad (47)$$

$$\text{C8FFAMAT}'[t] == \frac{\text{vacotC8} - \text{vmcFFAC8}}{\text{VMAT}} \quad (48)$$

$$\text{C6FFAMAT}'[t] == \frac{\text{vacotC6} - \text{vmcFFAC6}}{\text{VMAT}} \quad (49)$$

$$\text{C4FFAMAT}'[t] == \frac{\text{vacotC4} - \text{vmcFFAC4}}{\text{VMAT}} \quad (50)$$

$$\text{HMGCoAMAT}'[t] == \frac{-\text{vhmgcl} + \text{vhmgcs2}}{\text{VMAT}} \quad (51)$$

$$\text{AcetoacetateMAT}'[t] == \frac{-\text{vbdh1} - \text{vExAcetoacetateMAT} + \text{vhmgcl}}{\text{VMAT}} \quad (52)$$

$$\text{BetahydroxybutyrateMAT}'[t] == \frac{\text{vbdh1} - \text{vExBOHB}}{\text{VMAT}} \quad (53)$$

$$\text{C16FFACYT}'[t] == \frac{-\text{vacsC16} - \text{vcmiFFAC16} - \text{vExFFAC16} + \text{vmcFFAC16}}{\text{VCYT}} \quad (54)$$

$$\text{C14FFACYT}'[t] == \frac{-\text{vacsC14} - \text{vcmiFFAC14} - \text{vExFFAC14} + \text{vmcFFAC14}}{\text{VCYT}} \quad (55)$$

$$\text{C12FFACYT}'[t] == \frac{-\text{vacsC12} - \text{vcmiFFAC12} - \text{vExFFAC12} + \text{vmcFFAC12}}{\text{VCYT}} \quad (56)$$

$$\text{C10FFACYT}'[t] == \frac{-\text{vacsC10} - \text{vcmiFFAC10} - \text{vExFFAC10} + \text{vmcFFAC10}}{\text{VCYT}} \quad (57)$$

$$\text{C8FFACYT}'[t] == \frac{-\text{vacsC8} - \text{vcmiFFAC8} - \text{vExFFAC8} + \text{vmcFFAC8}}{\text{VCYT}} \quad (58)$$

$$\text{C6FFACYT}'[t] == \frac{-\text{vacsC6} - \text{vcmiFFAC6} - \text{vExFFAC6} + \text{vmcFFAC6}}{\text{VCYT}} \quad (59)$$

$$\text{C4FFACYT}'[t] == \frac{-\text{vacsC4} - \text{vcmiFFAC4} - \text{vExFFAC4} + \text{vmcFFAC4}}{\text{VCYT}} \quad (60)$$

$$\text{C14AcylCoACYT}'[t] == \frac{\text{vacsC14} - \text{vcpt1C14}}{\text{VCYT}} \quad (61)$$

$$\text{C12AcylCoACYT}'[t] == \frac{\text{vacsC12} - \text{vcpt1C12}}{\text{VCYT}} \quad (62)$$

$$\text{C10AcylCoACYT}'[t] == \frac{\text{vacsC10} - \text{vcpt1C10}}{\text{VCYT}} \quad (63)$$

$$\text{C8AcylCoACYT}'[t] == \frac{\text{vacsC8} - \text{vcpt1C8}}{\text{VCYT}} \quad (64)$$

$$\text{C6AcylCoACYT}'[t] == \frac{\text{vacsC6} - \text{vcpt1C6}}{\text{VCYT}} \quad (65)$$

$$\text{C4AcylCoACYT}'[t] == \frac{\text{vacsC4} - \text{vcpt1C4}}{\text{VCYT}} \quad (66)$$

$$\text{C16FFAMICR}'[t] == \frac{\text{vcmiFFAC16} - \text{v}\omega\text{oxC16}}{\text{VMICR}} \quad (67)$$

$$\text{C14FFAMICR}'[t] == \frac{\text{vcmiFFAC14} - \text{v}\omega\text{oxC14}}{\text{VMICR}} \quad (68)$$

$$\text{C12FFAMICR}'[t] == \frac{\text{vcmiFFAC12} - \text{v}\omega\text{oxC12}}{\text{VMICR}} \quad (69)$$

$$\text{C10FFAMICR}'[t] == \frac{\text{vcmiFFAC10} - \text{v}\omega\text{oxC10}}{\text{VMICR}} \quad (70)$$

$$\text{C8FFAMICR}'[t] == \frac{\text{vcmiFFAC8} - \text{v}\omega\text{oxC8}}{\text{VMICR}} \quad (71)$$

$$\text{C6FFAMICR}'[t] == \frac{\text{vcmiFFAC6} - \text{v}\omega\text{oxC6}}{\text{VMICR}} \quad (72)$$

$$\mathrm{C4FFAMICR}'[t] == \frac{\mathrm{vcmiFFAC4} - \mathrm{v\omega oxC4}}{\mathrm{VMICR}} \quad (73)$$

$$\mathrm{C16DCAMICR}'[t] == \frac{-\mathrm{vmicDCAC16} + \mathrm{v\omega oxC16}}{\mathrm{VMICR}} \quad (74)$$

$$\mathrm{C14DCAMICR}'[t] == \frac{-\mathrm{vmicDCAC14} + \mathrm{v\omega oxC14}}{\mathrm{VMICR}} \quad (75)$$

$$\mathrm{C12DCAMICR}'[t] == \frac{-\mathrm{vmicDCAC12} + \mathrm{v\omega oxC12}}{\mathrm{VMICR}} \quad (76)$$

$$\mathrm{C10DCAMICR}'[t] == \frac{-\mathrm{vmicDCAC10} + \mathrm{v\omega oxC10}}{\mathrm{VMICR}} \quad (77)$$

$$\mathrm{C8DCAMICR}'[t] == \frac{-\mathrm{vmicDCAC8} + \mathrm{v\omega oxC8}}{\mathrm{VMICR}} \quad (78)$$

$$\mathrm{C6DCAMICR}'[t] == \frac{-\mathrm{vmicDCAC6} + \mathrm{v\omega oxC6}}{\mathrm{VMICR}} \quad (79)$$

$$\mathrm{C4DCAMICR}'[t] == \frac{-\mathrm{vmicDCAC4} + \mathrm{v\omega oxC4}}{\mathrm{VMICR}} \quad (80)$$

$$\mathrm{C16DCACYT}'[t] == \frac{-\mathrm{vExDCAC16} + \mathrm{vmicDCAC16}}{\mathrm{VCYT}} \quad (81)$$

$$\mathrm{C14DCACYT}'[t] == \frac{-\mathrm{vExDCAC14} + \mathrm{vmicDCAC14}}{\mathrm{VCYT}} \quad (82)$$

$$\mathrm{C12DCACYT}'[t] == \frac{-\mathrm{vExDCAC12} + \mathrm{vmicDCAC12}}{\mathrm{VCYT}} \quad (83)$$

$$\mathrm{C10DCACYT}'[t] == \frac{-\mathrm{vExDCAC10} + \mathrm{vmicDCAC10}}{\mathrm{VCYT}} \quad (84)$$

$$\mathrm{C8DCACYT}'[t] == \frac{-\mathrm{vExDCAC8} + \mathrm{vmicDCAC8}}{\mathrm{VCYT}} \quad (85)$$

$$\mathrm{C6DCACYT}'[t] == \frac{-\mathrm{vExDCAC6} + \mathrm{vmicDCAC6}}{\mathrm{VCYT}} \quad (86)$$

$$\mathrm{C4DCACYT}'[t] == \frac{-\mathrm{vExDCAC4} + \mathrm{vmicDCAC4}}{\mathrm{VCYT}} \quad (87)$$

Rate equations

Most of the enzymes in this model catalyze reactions of substrates of more than one chain length. For such reactions the rate equations remain the same. In such cases, the general rate equation was given, where n indicates the carbon-chain length of a substrate. The parameters in the equations are most often chain-length-specific, as indicated in the subscript to the parameter (e.g. $Km_{cpt1C16AcylCoACYT}$ denoting the K_m of the enzyme CPT1 towards an acyl-CoA substrate with an acyl chain containing 16 carbon atoms, localized in the cytosol). Most equations are of the 2-substrate reversible Michaelis-Menten type or in exceptional cases based on mass-action kinetics. The reaction rates in the model are expressed in $\mu mol \cdot min^{-1} \cdot mgmitochondrialProtein^{-1}$, and the rate of metabolite concentration change in the ODEs are expressed as $\mu M \cdot min^{-1}$. In the model, the cofactors, CoQ, $CoQH_2$, NAD^+, NADH and acetyl-CoA are considered external/boundary parameters and have been fixed directly. This is in contrast to the Eunen *et al*. 2013 model, where acetyl-CoA and the cofactors in that model had been fixed indirectly via a sink reaction that had no flux control, but contained a parameter that effectively fixed these entities. Directly fixing these metabolites improves the stability of the model and decreases the stiffness of the ODEs. In the rate equations, the V_{max} values are denoted as V, and the carbon-chain length of substrates or products are given by n. K_m values denote the affinity of the enzyme for the indicated reactant, K_i values are inhibition constant of the enzyme for the indicated metabolite, and K_{eq} values denote the equilibrium constant of the reaction. Additional abbreviations are:

sf	Specificity factor. Multiplying the sf with $V_{max\ of\ the\ enzyme}$ will give the chain-length-specific V_{max} of that enzyme
ncpt1	Hill coefficient of for the cooperative inhibition of CPT1 by malonyl-CoA
NADt	Total concentration of oxidized and reduced NAD in the indicated organelle
CoAt	Total concentration free CoA and CoA esters in the indicated organelle
Car	Carnitine
CPT1	Carnitine-palmitoyl transferase 1
CACT	Carnitine-acyl-carnitine translocase
CPT2	Carnitine-palmitoyl transferase 2
SCAD	Short-chain acyl-CoA dehydrogenase
MCAD	Medium-chain acyl-CoA dehydrogenase
VLCAD	Very-long-chain acyl-CoA dehydrogenase
CROT	Crotonase or Enoyl Coenzyme A Hydratase
M/SCHAD	Medium/short-chain hydroxyacyl-CoA dehydrogenase
MCKAT	Medium-chain ketoacyl-CoA thiolase
MTP	Mitochondrial trifunctional protein
ETFQO	ETF dehydrogenase or ETF quinone oxidoreductase

ACAT1	Acetyl-CoA acetyltransferase 1 (mitochondrial) or Acetoacetyl-CoA thiolase
HMGCS2	3-hydroxy-3-methylglutaryl-CoA synthase 2 (mitochondrial)
HMGCL	3-hydroxy-3-methylglutaryl-CoA lyase or HMG-CoA lyase
BDH1	D-beta-hydroxybutyrate dehydrogenase (mitochondrial)
ACOT	Acyl-CoA thioesterase
ACS	Acyl-CoA synthetase
ωox	ω-oxidation of which the rate is represented by the rate of putative rate-limiting hydroxylation reaction catalyzed by CYP4A11
vExAccCn	Export rate of acyl-carnitine of chain length n from the cytosol into the blood
vmcFFACn	Translocation rate of free fatty acids of chainlength n from the mitochondrion to the cytosol
vExAcetoacetate	Export rate of acetoacetate
vExBOHB	Export rate of β-hydroxybutyrate
vExFFACn	Export rate of free fatty acids
vcmiFFACn	Translocation rate of free fatty acids from the cytosol to the microsome
vmicDCACn	Translocation rate of dicarboxylic acids from the microsome to the cytosol
vExDCACn	Export rate of dicarboxylic acids

Except for the rate equations for CACT, MTP, CROT and M/SCHAD, all rate equations are either new, due to added reactions, or adapted. Adaptations included humanization of parameters and expansion to accommodate chain-length-specific parameter values. For example, chain-length-specific K_m for L-carnitine was included for CPT1 as was chain-length-specific K_m for CoASH for MCKAT.

$$vcpt1Cn = \frac{sfcpt1Cn \cdot Vcpt1\left(\frac{CnAcylCoACYT \cdot CarCYT}{Kmcpt1CnAcylCoACYT \cdot Kmcpt1CarCYT} - \frac{CnAcylCarCYT[t] \cdot CoACYT}{Keqcpt1 \cdot Kmcpt1CnAcylCoACYT \cdot Kmcpt1CarCYT}\right)}{\left(1+\frac{CarCYT}{Kmcpt1CarCYT}+\frac{CoACYT}{Kmcpt1CoACYT}\right)\left(1+\frac{C16AcylCoACYT}{Kmcpt1C16AcylCoACYT}+\left(\frac{MalCoACYT}{Kicpt1 \cdot MalCoACYT}\right)^{ncpt1}+\sum_{n=4}^{n=14}\left(\frac{CnAcylCarCYT[t]}{Kmcpt1CnAcylCarCYT}+\frac{CnAcylCoACYT[t]}{Kmcpt1CnAcylCoACYT}\right)\right)} \quad (88)$$

$$vcactCn = \frac{sfcactCn \cdot Vfcact \cdot \left(CarMAT \cdot CnAcylCarCYT[t] - \frac{CarCYT \cdot CnAcylCarMAT[t]}{Keqcact}\right)}{CarMAT \cdot \left(1+\frac{CarCYT}{KicactCarCYT}\right) \cdot Kmcact CnAcylCarCYT + CarMAT \cdot CnAcylCarCYT[t] + Kmcact CarMAT \cdot CnAcylCarCYT[t] + \frac{Kmcact CarCYT \cdot \left(1+\frac{CnAcylCarCYT[t]}{Kicact \cdot CnAcylCarCYT}\right) \cdot CnAcylCarMAT[t] + CarCYT \cdot (Kmcact CnAcylCarMAT + CnAcylCarMAT[t])}{fVcact \cdot Keqcact}} \quad (89)$$

$$vcpt2Cn = \frac{sfcpt2Cn \cdot Vcpt2\left(\frac{CoAMAT \cdot C16AcylCarMAT[t]}{Kmcpt2C16AcylCarMAT \cdot Kmcpt2CoAMAT} - \frac{CarMAT \cdot C16AcylCoAMAT[t]}{Keqcpt2 \cdot Kmcpt2C16AcylCarMAT \cdot Kmcpt2CoAMAT}\right)}{\left(1+\frac{CarMAT}{Kmcpt2CarMAT}+\frac{CoAMAT}{Kmcpt2CoAMAT}\right)\left(1+\sum_{n=4}^{n=16}\left(\frac{CnAcylCarMAT[t]}{Kmcpt2CnAcylCarMAT}+\frac{CnAcylCoAMAT[t]}{Kmcpt2CnAcylCoAMAT}\right)\right)} \quad (90)$$

$$vvlcadCn = \frac{sfvlcadCn \cdot Vvlcad\left(\frac{CnAcylCoAMAT[t] \cdot (ETFtMAT - ETFhqMAT[t])}{KmvlcadCnAcylCoAMAT \cdot KmvlcadETFox} - \frac{CnEnoylCoAMAT[t] \cdot ETFhqMAT[t]}{Keqvlcad \cdot KmvlcadCnAcylCoAMAT \cdot KmvlcadETFox}\right)}{\left(1+\frac{ETFtMAT - ETFhqMAT[t]}{KmvlcadETFox}+\frac{ETFhqMAT[t]}{KmvlcadETFhq}\right) \cdot \left(1+\sum_{n=6}^{n=16}\left(\frac{CnAcylCoAMAT[t]}{KmvlcadCnAcylCoAMAT}+\frac{CnEnoylCoAMAT[t]}{KmvlcadCnEnoylCoAMAT}\right)\right)} \quad (91)$$

$$\text{vmcadCn} = \frac{\text{sfmcadCn}\cdot\text{Vmcad}\left(\frac{\text{CnAcylCoAMAT}[t]\cdot(\text{ETFtMAT}-\text{ETFhqMAT}[t])}{\text{KmmcadCnAcylCoAMAT}\cdot\text{KmmcadETFox}}-\frac{\text{CnEnoylCoAMAT}[t]\cdot\text{ETFhqMAT}[t]}{\text{Keqmcad}\cdot\text{KmmcadCnAcylCoAMAT}\cdot\text{KmmcadETFox}}\right)}{\left(1+\frac{\text{ETFtMAT}-\text{ETFhqMAT}[t]}{\text{KmmcadETFox}}+\frac{\text{ETFhqMAT}[t]}{\text{KmmcadETFhq}}\right)\cdot\left(1+\sum_{n=4}^{n=16}\left(\frac{\text{CnAcylCoAMAT}[t]}{\text{KmmcadCnAcylCoAMAT}}+\frac{\text{CnEnoylCoAMAT}[t]}{\text{KmmcadCnEnoylCoAMAT}}\right)\right)} \quad (92)$$

$$\text{vscadCn} = \frac{\text{sfmscadCn}\cdot\text{Vscad}\left(\frac{\text{CnAcylCoAMAT}[t]\cdot(\text{ETFtMAT}-\text{ETFhqMAT}[t])}{\text{KmscadCnAcylCoAMAT}\cdot\text{KmscadETFox}}-\frac{\text{CnEnoylCoAMAT}[t]\cdot\text{ETFhqMAT}[t]}{\text{Keqscad}\cdot\text{KmscadCnAcylCoAMAT}\cdot\text{KmscadETFox}}\right)}{\left(1+\frac{\text{ETFtMAT}-\text{ETFhqMAT}[t]}{\text{KmscadETFox}}+\frac{\text{ETFhqMAT}[t]}{\text{KmscadETFhq}}\right)\cdot\left(1+\sum_{n=4}^{n=6}\left(\frac{\text{CnAcylCoAMAT}[t]}{\text{KmscadCnAcylCoAMAT}}+\frac{\text{CnEnoylCoAMAT}[t]}{\text{KmscadCnEnoylCoAMAT}}\right)\right)} \quad (93)$$

$$\text{vcrotCn} = \frac{\text{sfcrotCn}\cdot\text{Vcrot}\cdot\left(\frac{\text{CnEnoylCoAMAT}[t]}{\text{KmcrotCnEnoylCoAMAT}}-\frac{\text{CnHydroxyacylCoAMAT}[t]}{\text{KeqcrotKmcrot}\cdot\text{CnEnoylCoAMAT}}\right)}{1+\frac{\text{AcetoacylCoAMAT}[t]}{\text{KicrotAcetoacylCoA}}+\sum_{n=4}^{n=16}\left(\frac{\text{CnEnoylCoAMAT}[t]}{\text{KmcrotCnEnoylCoAMAT}}+\frac{\text{CnHydroxyacylCoAMAT}[t]}{\text{KmcrotCnHydroxyacylCoAMAT}}\right)} \quad (94)$$

$$\text{vmschadCn} = \frac{\text{sfmschadCn}\cdot\text{Vmschad}\left(\frac{(-\text{NADHMAT}+\text{NADtMAT})\cdot\text{CnHydroxyacylCoAMAT}[t]}{\text{KmmschadCnHydroxyacylCoAMAT}\cdot\text{KmmschadNADMAT}}-\frac{\text{NADHMAT}\cdot\text{CnKetoacylCoAMAT}[t]}{\text{Keqmschad}\cdot\text{KmmschadCnHydroxyacylCoAMAT}\cdot\text{KmmschadNADMAT}}\right)}{\left(1+\frac{\text{NADHMAT}}{\text{KmmschadNADHMAT}}+\frac{-\text{NADHMAT}+\text{NADtMAT}}{\text{KmmschadNADMAT}}\right)\cdot\left(1+\sum_{n=4}^{n=16}\left(\frac{\text{CnHydroxyacylCoAMAT}[t]}{\text{KmmschadCnHydroxyacylCoAMAT}}+\frac{\text{CnKetoacylCoAMAT}[t]}{\text{KmmschadCnKetoacylCoAMAT}}\right)\right)} \quad (95)$$

$$\text{vmckatCn} = \frac{\text{sfmckatCn}\cdot\text{Vmckat}\cdot\left(\frac{\text{CoAMAT}\cdot\text{CnKetoacylCoAMAT}[t]}{\text{KmmckatCnKetoacylCoAMAT}\cdot\text{KmmckatCoAMATCn}}-\frac{\text{AcetylCoAMATCn-2AcylCoAMAT}[t]}{\text{Keqmckat}\cdot\text{KmmckatCnKetoacylCoAMAT}\cdot\text{KmmckatCoAMATCn}}\right)}{\left(1+\frac{\text{AcetylCoAMAT}}{\text{KmmckatAcetylCoAMAT}}+\frac{\text{CoAMAT}}{\text{KmmckatCoAMATCn}}\right)\cdot\left(1+\frac{\text{AcetylCoAMAT}}{\text{KmmckatAcetylCoAMAT}}+\sum_{n=4}^{n=16}\left(\frac{\text{Cn-2AcylCoAMAT}[t]}{\text{KmmckatCn-2AcylCoAMAT}}+\frac{\text{CnKetoacylCoAMAT}[t]}{\text{KmmckatCnKetoacylCoAMAT}}\right)\right)} \quad (96)$$

$$\text{vmtpCn} = \cdot\frac{\text{sfmtpC16}\cdot\text{Vmtp}\left(-\frac{\text{AcetylCoAMAT}\cdot\text{NADHMAT}\cdot\text{C14AcylCoAMAT}[t]}{\text{Keqmtp}\cdot\text{KmmtpC16EnoylCoAMAT}\cdot\text{KmmtpCoAMAT}\cdot\text{KmmtpNADMAT}}+\frac{\text{CoAMAT}\cdot(-\text{NADHMAT}+\text{NADtMAT})\cdot\text{C16EnoylCoAMAT}[t]}{\text{KmmtpC16EnoylCoAMAT}\cdot\text{KmmtpCoAMAT}\cdot\text{KmmtpNADMAT}}\right)}{\left(1+\frac{\text{AcetylCoAMAT}}{\text{KmmtpAcetylCoAMAT}}+\frac{\text{CoAMAT}}{\text{KmmtpCoAMAT}}\right)\cdot\left(1+\frac{\text{NADHMAT}}{\text{KmmtpNADHMAT}}+\frac{-\text{NADHMAT}+\text{NADtMAT}}{\text{KmmtpNADMAT}}\right)\cdot\left(1+\sum_{n=8}^{n=16}\left(\frac{\text{Cn-2AcylCoAMAT}[t]}{\text{KmmtpCn-2AcylCoAMAT}}+\frac{\text{CnEnoylCoAMAT}[t]}{\text{KmmtpCnEnoylCoAMAT}}\right)\right)} \quad (97)$$

$$\text{vetfqo} = \frac{\text{Vfetfqo}\cdot\left(-\frac{\text{CoQH2}(\text{ETFtMAT}-\text{ETFhqMAT}[t])}{\text{KeqEtfqo}}+(\text{CoQt}-\text{CoQH2})\cdot\text{ETFhqMAT}[t]\right)}{(-\text{CoQH2}+\text{CoQt})\cdot\left(1+\frac{\text{CoQH2}}{\text{KiEtfqoCoQH2}}\right)\cdot\text{KmEtfqoEtfhq}+(-\text{CoQH2}+\text{CoQt})\cdot\text{ETFhqMAT}[t]+\text{KmEtfqoCoQ}\cdot\text{ETFhqMAT}[t]} \quad (98)$$
$$+\frac{\text{CoQH2}\cdot(\text{ETFtMAT}+\text{KmEtfqoEtfox}-\text{ETFhqMAT}[t])+\text{KmEtfqoCoQH2}\cdot(\text{ETFtMAT}-\text{ETFhqMAT}[t])\cdot\left(1+\frac{\text{ETFhqMAT}[t]}{\text{KiEtfqoEtfhq}}\right)}{\text{KeqEtfqo}}$$

$$\text{vacotCn} = \frac{\text{sfacotCn}\cdot\text{Vacot}\cdot\left(\frac{\text{CnAcylCoAMAT}[t]}{\text{KmacotCnAcylCoAMAT}}-\frac{\text{CoAMAT}\cdot\text{CnFFAMAT}[t]}{\text{KeqacotCnAcylCoA}\cdot\text{KmacotCnAcylCoAMAT}}\right)}{\left(1+\frac{\text{CoAMAT}}{\text{KmacotCoAMAT}}\right)\left(1+\sum_{n=4}^{n=16}\left(\frac{\text{CnAcylCoAMAT}[t]}{\text{KmacotCnAcylCoAMAT}}+\frac{\text{CnFFAMAT}[t]}{\text{KmacotCnFFAMAT}}\right)\right)} \quad (99)$$

$$\text{vExCn} = \text{keCn}\cdot\text{CnAcylCarCYT}[t] \quad (100)$$

$$\text{vmcFFACn} = \text{kmc}\cdot(\text{CnFFAMAT}[t]-\text{CnFFACYT}[t]) \quad (101)$$

$$\text{vacat1} = -\frac{\text{Vacat1}\cdot\left(\frac{\text{CoAMAT}\cdot\text{C4AcetoacylCoAMAT}[t]}{\text{Kmacat1C4AcetoacylCoAMAT}\cdot\text{Kmacat1CoAMAT}}-\frac{\text{AcetylCoAMAT}^2}{\text{Keqacat1}\cdot\text{Kmacat1C4AcetoacylCoAMAT}\cdot\text{Kmacat1CoAMAT}}\right)}{\left(1+\frac{\text{AcetylCoAMAT}}{\text{Kmacat1AcetylCoAMAT}}+\frac{\text{CoAMAT}}{\text{Kmacat1CoAMAT}}\right)\cdot\left(1+\frac{\text{AcetylCoAMAT}}{\text{Kmacat1AcetylCoAMAT}}+\frac{\text{C4AcetoacylCoAMAT}[t]}{\text{Kmacat1C4AcetoacylCoAMAT}}\right)} \quad (102)$$

$$\text{vhmgcs2} = \frac{\text{Vhmgcs2}\left(\frac{\text{AcetylCoAMATC4AcetoacylCoAMAT}[t]}{\text{Kmhmgcs2AcetylCoAMATKmhmgcs2C4AcetoacylCoAMAT}} - \frac{\text{CoAMATHMGCoAMAT}[t]}{\text{Keqhmgcs2Kmhmgcs2AcetylCoAMATKmhmgcs2C4AcetoacylCoAMAT}}\right)}{\left(1+\frac{\text{AcetylCoAMAT}}{\text{Kmhmgcs2AcetylCoAMAT}}+\frac{\text{CoAMAT}}{\text{Kmhmgcs2CoAMAT}}\right)\left(1+\frac{\text{C4AcetoacylCoAMAT}[t]}{\text{Kmhmgcs2C4AcetoacylCoAMAT}}+\frac{\text{HMGCoAMAT}[t]}{\text{Kmhmgcs2HMGCoAMAT}}\right)} \quad (103)$$

$$\text{vhmgcl} = \frac{\text{Vhmgcl}\cdot\left(\frac{\text{HMGCoAMAT}[t]}{\text{Kmhmgcl HMGCoAMAT}} - \frac{\text{AcetylCoAMAT}\cdot\text{AcetoacetateMAT}[t]}{\text{Keqhmgcl}\cdot\text{Kmhmgcl HMGCoAMAT}}\right)}{1+\frac{\text{AcetylCoAMAT}}{\text{KmhmgclAcetylCoAMAT}}+\frac{\text{AcetoacetateMAT}[t]}{\text{KmhmgclAcetoacetateMAT}}+\frac{\text{AcetylCoAMAT}\cdot\text{AcetoacetateMAT}[t]}{\text{KmhmgclAcetoacetateMAT}\cdot\text{KmhmgclAcetylCoAMAT}}+\frac{\text{HMGCoAMAT}[t]}{\text{KmhmgclHMGCoAMAT}}+\frac{\text{AcetoacetateMAT}[t]\cdot\text{HMGCoAMAT}[t]}{\text{KmhmgclAcetoacetateMAT}\cdot\text{KmhmgclHMGCoAMAT}}} \quad (104)$$

$$\text{vExAcetoacetateMAT} = \text{keAcetoacetateMAT}\cdot\text{AcetoacetateMAT}[t] \quad (105)$$

The BDH1-catalyzed reaction is according to the Ordered Bi Bi equation:

$$\text{vbdh1} = -\frac{\text{Vbdh1}\left(-\frac{\text{NADHMATAcetoacetateMAT}[t]}{\text{Keqbdh1}\cdot\text{Kibdh1NADMAT}\cdot\text{Kmbdh1BetahydroxybutyrateMAT}}+\frac{(-\text{NADHMAT}+\text{NADtMAT})\cdot\text{BetahydroxybutyrateMAT}[t]}{\text{Kibdh1NADMAT}\cdot\text{Kmbdh1BetahydroxybutyrateMAT}}\right)}{\begin{aligned}&1+\frac{\text{NADHMAT}}{\text{Kibdh1NADHMAT}}+\frac{-\text{NADHMAT}+\text{NADtMAT}}{\text{Kibdh1NADMAT}}+\frac{\text{Kmbdh1NADHMAT}\cdot\text{AcetoacetateMAT}[t]}{\text{Kmbdh1AcetoacetateMAT}}+\frac{\text{NADHMAT}\cdot\text{AcetoacetateMAT}[t]}{\text{Kibdh1NADHMAT}\cdot\text{Kmbdh1AcetoacetateMAT}}\\&+\frac{\text{Kmbdh1NADHMAT}\cdot(-\text{NADHMAT}+\text{NADtMAT})\cdot\text{AcetoacetateMAT}[t]}{\text{Kibdh1NADHMAT}\cdot\text{Kibdh1NADMAT}\cdot\text{Kmbdh1AcetoacetateMAT}}+\frac{\text{Kmbdh1NADMAT}\cdot\text{BetahydroxybutyrateMAT}[t]}{\text{Kibdh1NADMAT}\cdot\text{Kmbdh1BetahydroxybutyrateMAT}}+\frac{\text{Kmbdh1NADMAT}\cdot\text{NADHMATBetahydroxybutyrateMAT}[t]}{\text{Kibdh1NADHMAT}\cdot\text{Kibdh1NADMAT}\cdot\text{Kmbdh1BetahydroxybutyrateMAT}}\\&+\frac{(-\text{NADHMAT}+\text{NADtMAT})\cdot\text{BetahydroxybutyrateMAT}[t]}{\text{Kibdh1NADMAT}\cdot\text{Kmbdh1BetahydroxybutyrateMAT}}+\frac{\text{NADHMATAcetoacetateMAT}[t]\cdot\text{BetahydroxybutyrateMAT}[t]}{\text{Kibdh1BetahydroxybutyrateMAT}\cdot\text{Kibdh1NADHMAT}\cdot\text{Kmbdh1AcetoacetateMAT}}+\frac{(-\text{NADHMAT}+\text{NADtMAT})\cdot\text{AcetoacetateMAT}[t]\cdot\text{BetahydroxybutyrateMAT}[t]}{\text{Kibdh1AcetoacetateMAT}\cdot\text{Kibdh1NADMAT}\cdot\text{Kmbdh1BetahydroxybutyrateMAT}}\end{aligned}} \quad (106)$$

$$\text{vExBOHB} = \text{keBetahydroxybutyrateMAT}\cdot\text{BetahydroxybutyrateMAT}[t] \quad (172)$$

$$\text{vExFFACn} = \text{keFFACn}\cdot\text{FFAMAT}[t] \quad (108)$$

The ACS reaction is modeled as an irreversible reaction. The rate equation is a Michaelis-Menten equation for an irreversible reaction with 3 substrates.

$$\text{vacsCn} = \frac{\text{sfacsCn}\cdot\text{Vacs}\cdot\text{CnFFACYT}[t]\cdot\text{ATPCYT}\cdot\text{CoACYT}}{\text{KmacsATPCYT}\cdot\text{KmacsCnFFACYT}\cdot\text{KmacsCoACYT}\cdot\left(\frac{\text{CoACYT}}{\text{KmacsCoACYT}}+\frac{\text{ATPCYT}\cdot\text{CoACYT}}{\text{KmacsATPCYT}\cdot\text{KmacsCoACYT}}+\left(\frac{\text{ATPCYT}}{\text{KmacsATPCYT}}+\frac{\text{CoACYT}}{\text{KmacsCoACYT}}+\frac{\text{ATPCYT}\cdot\text{CoACYT}}{\text{KmacsATPCYT}\cdot\text{KmacsCoACYT}}\right)\cdot\left(\sum_{n=4}^{n=16}\left(\frac{\text{CnFFACYT}[t]}{\text{KmacsCnFFACYT}}\right)\right)\right)} \quad (109)$$

$$\text{vcmiFFACn} = \text{kcmi}\cdot(\text{CnFFACYT}[t]-\text{CnFFAMICR}[t]) \quad (110)$$

$$\text{vwoxCn} = \frac{\text{Vwox}\cdot\text{CnFFAMICR}[t]\cdot\text{NADPHMICR}\cdot\text{sfwoxCn}}{\text{KmwoxCnFFAMICR}\cdot\text{KmwoxNADPHMICR}\cdot\left(1+\frac{\text{NADPHMICR}}{\text{KmwoxNADPHMICR}}\right)\cdot\left(1+\sum_{n=4}^{n=16}\frac{\text{CnFFAMICR}[t]}{\text{KmwoxCnFFAMICR}}\right)} \quad (111)$$

$$\mathrm{vmicDCACn} = \mathrm{kmic} \cdot (-\mathrm{CnDCACYT}[t] + \mathrm{CnDCAMICR}[t]) \quad (112)$$

$$\mathrm{vExDCACn} = \mathrm{keDCACn} \cdot \mathrm{DCACYT}[t] \quad (113)$$

Conserved moiety equations

$$\{\mathrm{CoAMAT} = \mathrm{CoAMATt} - \mathrm{C16AcylCoAMAT[t]} - \mathrm{C16EnoylCoAMAT[t]} - \mathrm{C16HydroxyacylCoAMAT[t]} - \mathrm{C16KetoacylCoAMAT[t]} - \mathrm{C14AcylCoAMAT[t]} - \mathrm{C14EnoylCoAMAT[t]} - \mathrm{C14HydroxyacylCoAMAT[t]} - \mathrm{C14KetoacylCoAMAT[t]} - \mathrm{C12AcylCoAMAT[t]} - \mathrm{C12EnoylCoAMAT[t]} - \mathrm{C12HydroxyacylCoAMAT[t]} - \mathrm{C12KetoacylCoAMAT[t]} - \mathrm{C10AcylCoAMAT[t]} - \mathrm{C10EnoylCoAMAT[t]} - \mathrm{C10HydroxyacylCoAMAT[t]} - \mathrm{C10KetoacylCoAMAT[t]} - \mathrm{C8AcylCoAMAT[t]} - \mathrm{C8EnoylCoAMAT[t]} - \mathrm{C8HydroxyacylCoAMAT[t]} - \mathrm{C8KetoacylCoAMAT[t]} - \mathrm{C6AcylCoAMAT[t]} - \mathrm{C6EnoylCoAMAT[t]} - \mathrm{C6HydroxyacylCoAMAT[t]} - \mathrm{C6KetoacylCoAMAT[t]} - \mathrm{C4AcylCoAMAT[t]} - \mathrm{C4EnoylCoAMAT[t]} - \mathrm{C4HydroxyacylCoAMAT[t]} - \mathrm{C4AcetoacylCoAMAT[t]} - \mathrm{AcetylCoAMAT} - \mathrm{HMGCoAMAT[t]}\} \quad (114)$$

Model parameters

The values of the parameters used for the model simulations are given in Table 1. Deviations from these values are given in the figure legends where applicable. The parametrization of the model was based on *in vitro* kinetic data of isolated enzymes or isolated organelle or computational modeling literature. Where a similar value was used as in Eunen *et al.* 2013 [1], this reference paper was given as reference.

Parameter	Value	unit	Used references
CPT1			
$sf_{cpt1C16}$	1		[3]
$sf_{cpt1C14}$	1.34		[3]
$sf_{cpt1C12}$	1.93		[3]
$sf_{cpt1C10}$	1.54		[3]
sf_{cpt1C8}	0.83		[3]
sf_{cpt1C6}	0.51		[3]
sf_{cpt1C4}	0.25		Estimated based on [3,4]
V_{cpt1}	0.028	µmol.min^{-1}.mgProtein^{-1}	Estimated based on [3,5,6]
$Km_{cpt1C16AcylCoACYT}$	12.2	µM	[3]
$Km_{cpt1C14AcylCoACYT}$	30.8	µM	[3]
$Km_{cpt1C12AcylCoACYT}$	11	µM	[3]
$Km_{cpt1C10AcylCoACYT}$	16.7	µM	[3]
$Km_{cpt1C8AcylCoACYT}$	22.9	µM	[3]
$Km_{cpt1C6AcylCoACYT}$	151.5	µM	[3]
$Km_{cpt1C4AcylCoACYT}$	653.5	µM	Extrapolated based [3,4]
$Km_{cpt1CarCYTC16}$	386	µM	[3]
$Km_{cpt1CarCYTC14}$	593	µM	[3]
$Km_{cpt1CarCYTC12}$	400	µM	[3]
$Km_{cpt1CarCYTC10}$	1554	µM	Intrapolated
$Km_{cpt1CarCYTC8}$	5014	µM	[3]
$Km_{cpt1CarCYTC6}$	16183	µM	[3]
$Km_{cpt1CarCYTC4}$	52231	µM	[3]
$Km_{cpt1C16AcylCarCYT}$	123	µM	[3]
$Km_{cpt1C14AcylCarCYT}$	377	µM	[3]
$Km_{cpt1C12AcylCarCYT}$	631	µM	[3]
$Km_{cpt1C10AcylCarCYT}$	885	µM	[3]
$Km_{cpt1C8AcylCarCYT}$	1139	µM	[3]
$Km_{cpt1C6AcylCarCYT}$	1393	µM	[3]
$Km_{cpt1C4AcylCarCYT}$	1647	µM	[3]
$Km_{cpt1CoACYT}$	40.7	µM	[1]
$Ki_{cpt1MalCoACYT}$	9.1	µM	[1]
Keq_{cpt1}	0.45		[1]
n_{cpt1}	2.4799		[1]
CACT			
$sf_{cact1Cn}$	1		[1]
Vf_{cact}	0.42	µmol.min^{-1}.mgProtein^{-1}	[1]
$Km_{CnAcylCarCYT}$	15	µM	[1]
Km_{CarMAT}	130	µM	[1]
$Km_{CnAcylCarMAT}$	15	µM	[1]
Km_{CarCYT}	130	µM	[1]
$Ki_{CnAcylCarCYT}$	56	µM	[1]
Ki_{CarCYT}	200	µM	[1]
Keq_{cact}	1		[1]

Parameter	Value	unit	References
CPT2			
$sf_{cpt2C16}$	0.85		Estimated based on [7,8]
$sf_{cpt2C14}$	1.00		Estimated based on [7,8]
$sf_{cpt2C12}$	0.96		Estimated based on [7,8]
$sf_{cpt2C10}$	1.00		Estimated based on [7,8]
sf_{cpt2C8}	0.42		Estimated based on [7,8]
sf_{cpt2C6}	0.25		Estimated based on [7,8]
sf_{cpt2C4}	0.19		Estimated based on [7,8]
V_{cpt2}	0.392	µmol.min^{-1}.mgProtein^{-1}	Estimated based on [7,8]
$Km_{cpt2C16AcylCarMAT}$	67.00	µM	Estimated based on [7,8]
$Km_{cpt2C14AcylCarMAT}$	4.60	µM	Estimated based on [7,8]
$Km_{cpt2C12AcylCarMAT}$	15	µM	Estimated based on [7,8]
$Km_{cpt2C10AcylCarMAT}$	43	µM	Estimated based on [7,8]
$Km_{cpt2C8AcylCarMAT}$	187.46	µM	Estimated based on [7,8]
$Km_{cpt2C6AcylCarMAT}$	125.54	µM	Estimated based on [7,8]
$Km_{cpt2C4AcylCarMAT}$	43.5	µM	Estimated based on [7,8]
$Km_{cpt2CoAMAT}$	30	µM	[1]
$Km_{cpt2C16AcylCoAMAT}$	6.3	µM	Estimated based on [7,8]
$Km_{cpt2C14AcylCoAMAT}$	7.8	µM	Estimated based on [7,8]
$Km_{cpt2C12AcylCoAMAT}$	22.4	µM	Estimated based on [7,8]
$Km_{cp2C10AcylCoAMAT}$	37	µM	Estimated based on [7,8]
$Km_{cpt2C8AcylCoAMAT}$	50.3	µM	Estimated based on [7,8]
$Km_{cpt2C6AcylCoAMAT}$	54.5	µM	Estimated based on [7,8]
$Km_{cpt2C4AcylCoAMAT}$	43.5	µM	[1]
$Km_{cpt2CarMAT}$	350	µM	[1]
Keq_{cpt2}	2.22		
VLCAD			
$sf_{vlcadC16}$	1.00		Estimated based on [6,9,10]
$sf_{vlcadC14}$	0.43		Estimated based on [6,9,10]
$sf_{vlcadC12}$	0.26		Estimated based on [6,9,10]
$sf_{vlcadC10}$	0.06		Estimated based on [6,9–11]
$sf_{vlcadC8}$	0.03		Estimated based on [6,9–11]
$sf_{vlcadC6}$	0.01		Estimated based on [6,9–11]
V_{vlcad}	0.103		Estimated based on [6,9–11]
$Km_{C16AcylCoAMAT}$	1.65	µmol.min^{-1}.mgProtein^{-1}	Estimated based on [11,12]
$Km_{C14AcylCoAMAT}$	1.15	µM	Estimated based on [11,12]
$Km_{C12AcylCoAMAT}$	0.80	µM	Estimated based on [11,12]
$Km_{C10AcylCoAMAT}$	10	µM	[10]
$Km_{C8AcylCoAMAT}$	8	µM	[10]
$Km_{C6AcylCoAMAT}$	29	µM	[10]
Km_{ETFoX}	0.12	µM	[1]
$Km_{CnEnoylCoAMAT}$	1.08	µM	[1]
Km_{ETFred}	24.2	µM	[1]
Keq_{vlcad}	6		[1]

Parameter	Value	unit	References
MCAD			
$sf_{mcadC16}$	0.016		Estimated based on [11,13]
$sf_{mcadC14}$	0.21		[13]
$sf_{mcadC12}$	0.45		[13]
$sf_{mcadC10}$	0.52		[13]
sf_{mcadC8}	0.75		[13]
sf_{mcadC6}	1.00		[13]
sf_{mcadC4}	0.14		[13]
V_{mcad}	0.074		Estimated based on [9,13]
$Km_{C16AcylCoAMAT}$	23.8	µmol.min^{-1}.mgProtein^{-1}	[13]
$Km_{C14AcylCoAMAT}$	10.0	µM	[13]
$Km_{C12AcylCoAMAT}$	9.3	µM	[13]
$Km_{C10AcylCoAMAT}$	9.1	µM	[13]
$Km_{C8AcylCoAMAT}$	8	µM	[13]
$Km_{C6AcylCoAMAT}$	21.6	µM	[13]
$Km_{C4AcylCoAMAT}$	71.4	µM	[13]
Km_{ETFox}	0.12	µM	[1]
$Km_{CnEnoylCoAMAT}$	1.08	µM	[1]
Km_{ETFred}	24.2	µM	[1]
Keq_{vlcad}	6		[1]
SCAD			
sf_{scadC6}	0.88		[13]
sf_{scadC4}	1		[13]
V_{scad}	0.060	µmol.min^{-1}.mgProtein^{-1}	Estimated based on [9,13]
$Km_{C6AcylCoAMAT}$	33.9	µM	[13]
$Km_{C4AcylCoAMAT}$	12.9	µM	[13]
Km_{ETFox}	0.12	µM	[1]
$Km_{CnEnoylCoAMAT}$	1.08	µM	[1]
Km_{ETFred}	24.2	µM	[1]
Keq_{scad}	6		[1]
CROT			[1]
$sf_{crotC16}$	0.13		[1]
$sf_{crotC14}$	0.2		[1]
$sf_{crotC12}$	0.25		[1]
$sf_{crotC10}$	0.33		[1]
sf_{crotC8}	0.58		[1]
sf_{crotC6}	0.8		[1]
sf_{crotC4}	1		[1]
V_{crot}	3.6	µmol.min^{-1}.mgProtein^{-1}	[1]
$Km_{C16EnoylCoAMAT}$	150	µM	[1]
$Km_{C14EnoylCoAMAT}$	100	µM	[1]
$Km_{C12EnoylCoAMAT}$	25	µM	[1]

Parameter	Value	unit	References
$Km_{C10EnoylCoAMAT}$	25	µM	[1]
$Km_{C8EnoylCoAMAT}$	25	µM	[1]
$Km_{C6EnoylCoAMAT}$	25	µM	[1]
$Km_{C4EnoylCoAMAT}$	40	µM	[1]
$Km_{CNHydroxyacylCoAMAT}$	45	µM	[1]
$Ki_{acetoacetylCoAMAT}$	1.6	µM	[1]
Keq_{crot}	3.13		[1]
MSCHAD			
$sf_{mschadC16}$	0.6		[1]
$sf_{mschadC14}$	0.5		[1]
$sf_{mschadC12}$	0.43		[1]
$sf_{mschadC10}$	0.64		[1]
$sf_{mschadC8}$	0.89		[1]
$sf_{mschadC6}$	1		[1]
$sf_{mschadC4}$	0.67		[1]
V_{mschad}	1	µmol.min^{-1}.mgProtein^{-1}	[1]
$Km_{C16HydroxyacylCoAMAT}$	1.5	µM	[1]
$Km_{C14HydroxyacylCoAMAT}$	1.8	µM	[1]
$Km_{C12HydroxyacylCoAMAT}$	3.7	µM	[1]
$Km_{C10HydroxyacylCoAMAT}$	8.8	µM	[1]
$Km_{C8HydroxyacylCoAMAT}$	16.3	µM	[1]
$Km_{C6HydroxyacylCoAMAT}$	28.6	µM	[1]
$Km_{C4HydroxyacylCoAMAT}$	69.9	µM	[1]
Km_{NADMAT}	58.5	µM	[1]
$Km_{C16KetoacylCoAMAT}$	1.4	µM	[1]
$Km_{C14KetoacylCoAMAT}$	1.4	µM	[1]
$Km_{C12KetoacylCoAMAT}$	1.6	µM	[1]
$Km_{C10KetoacylCoAMAT}$	2.3	µM	[1]
$Km_{C8KetoacylCoAMAT}$	4.1	µM	[1]
$Km_{C6KetoacylCoAMAT}$	5.8	µM	[1]
$Km_{C4AcetoacylCoAMAT}$	16.9	µM	[1]
$Km_{NADHMAT}$	5.4	µM	[1]
Keq_{mschad}	$2.17 \cdot 10^{-4}$		[1]
MCKAT			
$sf_{mckatC16}$	0.01		Arbitrary non-zero value
$sf_{mckatC14}$	0.2		[1]
$sf_{mckatC12}$	0.38		[1]
$sf_{mckatC10}$	0.65		[1]
$sf_{mckatC8}$	0.81		[1]
$sf_{mckatC6}$	1		[1]
$sf_{mckatC4}$	0.49		[1]
V_{mckat}	0.463	µmol.min^{-1}.mgProtein^{-1}	Estimated based on [6,14]
$Km_{mckatC16KetoacylCoAMAT}$	0.5	µM	Estimated based on [14,15]

Parameter	Value	unit	References
$Km_{mckatC14KetoacylCoAMAT}$	0.55	µM	Estimated based on [14,15]
$Km_{mckatC12KetoacylCoAMAT}$	0.6	µM	Estimated based on [14,15]
$Km_{mckatC10KetoacylCoAMAT}$	0.97	µM	Estimated based on [14,15]
$Km_{mckatC8KetoacylCoAMAT}$	1.29	µM	Estimated based on [14,15]
$Km_{mckatC6KetoacylCoAMAT}$	4.45	µM	Estimated based on [14,15]
$Km_{mckatC4AcetoacetylCoAMAT}$	9.2	µM	[14]
$Km_{mckatCoAMATC16}$	113.1	µM	Estimated based on [15,16]
$Km_{mckatCoAMATC14}$	132.5	µM	Estimated based on [15,16]
$Km_{mckatCoAMATC12}$	151.9	µM	Estimated based on [15,16]
$Km_{mckatCoAMATC10}$	141.2	µM	Estimated based on [15,16]
$Km_{mckatCoAMATC8}$	140.4	µM	Estimated based on [15,16]
$Km_{mckatCoAMATC6}$	74.7	µM	Estimated based on [15,16]
$Km_{mckatCoAMATC4}$	8.7	µM	[15]
$Km_{mckatC16AcylCoAMAT}$	65.6	µM	Estim. using Haldane Rel. w. Vf/Vr=10
$Km_{mckatC14AcylCoAMAT}$	65.6	µM	Estim. using Haldane Rel. w. Vf/Vr=10
$Km_{mckatC12AcylCoAMAT}$	83.8	µM	Estim. using Haldane Rel. w. Vf/Vr=10
$Km_{mckatC10AcylCoAMAT}$	104	µM	Estim. using Haldane Rel. w. Vf/Vr=10
$Km_{mckatC8AcylCoAMAT}$	156.2	µM	Estim. using Haldane Rel. w. Vf/Vr=10
$Km_{mckatC6AcylCoAMAT}$	207.1	µM	Estim. using Haldane Rel. w. Vf/Vr=10
$Km_{mckatC4AcylCoAMAT}$	381.3	µM	Estim. using Haldane Rel. w. Vf/Vr=10
$Km_{mckatAcetylCoAMAT}$	91.7	µM	Estim. using Haldane Rel. w. Vf/Vr=10
Keq_{mckat}	1051		[1]
MTP			
sf_{mtpC16}	1		[1]
sf_{mtpC14}	0.9		[1]
sf_{mtpC12}	0.81		[1]
sf_{mtpC10}	0.73		[1]
sf_{mtpC8}	0.34		[1]
V_{mtp}	2.84	µmol.min^{-1}.mgProtein^{-1}	[1]
$Km_{CnEnoylCoAMAT}$	25	µM	[1]
Km_{NADMAT}	60	µM	[1]
Km_{CoAMAT}	30	µM	[1]
$Km_{CnAcylCoAMAT}$	13.83	µM	[1]
$Km_{NADHMAT}$	50	µM	[1]
$Km_{AcetylCoAMAT}$	30	µM	[1]
Keq_{mtp}	0.71		[1]
ETFQO			
V_{etfqo}	0.0735	µmol.min^{-1}.mgProtein^{-1}	Estimated based on [6,17,18]
$Km_{EtfqoEtfhq}$	1.97	µM	[17]
$Km_{EtfqoCoQ}$	20.3	µM	Estimated based on [17,19]
$Km_{EtfqoEtfox}$	1.97	µM	Estimated based on [17,20]
$Km_{EtfqoCoQH2}$	38.1	µM	Estim. using Haldane Rel. with Vf/Vr=1

Parameter	Value	unit	References
$Ki_{EtfqoEtfhq}$	1.97	µM	Assumed equal to $Km_{EtfqoEtfhq}$
$Ki_{EtfqoCoQH2}$	38.1	µM	Assumed equal to $Km_{EtfqoCoQH2}$
Keq_{Etfqo}	199.5		Estimated based on [21,22]
ACAT1			
V_{ACAT1}	0.349	µmol.min^{-1}.mgProtein^{-1}	Estimated based on [5,6]
$Km_{ACAT1,AcetylCoAMAT}$	6.2	µM	[23]
$Km_{ACAT1,AcetoacetylCoAMAT}$	7	µM	[24]
$Km_{ACAT1,CoAMAT}$	21	µM	[24]
Keq_{ACAT1}	1051		[1] (in the thiolase direction)
HMGCS2			
V_{HMGCS2}	0.021	µmol.min^{-1}.mgProtein^{-1}	[25]
$Km_{Hmgcs2C4AcetoacylCoAMAT}$	0.35	µM	
$Km_{hmgcs2AcetylCoAMAT}$	51	µM	[26]
$Km_{hmgcs2HMGCoAMAT}$	35	µM	[26]
$Km_{hmgcs2CoAMAT}$	500	µM	[26]
Keq_{HMGCS2}	3000		[27]
HMGCL			
Vf_{HMGCL}	0.133	µmol.min^{-1}.mgProtein^{-1}	[25]
$Km_{hmgclHMGCoAMAT}$	8	µM	[28]
$Km_{hmgclAcetylCoAMAT}$	30	µM	Assumed same as MCKAT
$Km_{hmgclAcetoacetateMAT}$	21	µM	[29]
Keq_{HMGCL}	2000	µM	[30]
BDH1			
V_{BDH1}	1.99	µmol.min^{-1}.mgProtein^{-1}	[31]
$Km_{bdh1AcetoacetateMAT}$	149	µM	[31]
$Km_{bdh1NADHMAT}$	14	µM	[31]
$Km_{bdh1BetahydroxybutyrateMAT}$	866	µM	[31]
$Km_{bdh1NADMAT}$	71	µM	[31]
$Ki_{bdh1AcetoacetateMAT}$	584	µM	[31]
$Ki_{bdh1NADHMAT}$	75	µM	[31]
$Ki_{bdh1BetahydroxybutyrateMAT}$	10000	µM	Assumed high based on [31]
$Ki_{bdh1NADMAT}$	301	µM	[31]
Keq_{bdh1}	1.255		Calculated with: (V1/V2)*((Kp*Kiq)/(Kia*Kb))
ACOT			
$sf_{acotC16}$	0.83		[32]
$sf_{acotC14}$	0.89		[32]

Parameter	Value	unit	References
$sf_{acotC12}$	1		[32]
$sf_{acotC10}$	0.47		[32]
sf_{acotC8}	0.51		[32]
sf_{acotC6}	0.26		[32]
sf_{acotC4}	0.047		[32]
V_{max_ref}	0.0437	$\mu mol.min^{-1}.mgProtein^{-1}$	[32–37]
$Km_{acotC16CoA}$	2.6	µM	[32]
$Km_{acotC14CoA}$	2.4	µM	[32]
$Km_{acotC10CoA}$	6.1	µM	[32]
$Km_{acotC8CoA}$	8.3	µM	[32]
$Km_{acotC6CoA}$	13	µM	[32]
$Km_{acotC4CoA}$	16	µM	[32]
$Km_{acotC16FFA}$	62400	µM	$Km_{acotCnCoA} \cdot Keq_{acotCn}$
$Km_{acotC14FFA}$	182400	µM	" "
$Km_{acotC12FFA}$	250800	µM	" "
$Km_{acotC10FFA}$	463600	µM	" "
$Km_{acotC8FFA}$	630800	µM	" "
$Km_{acotC6FFA}$	988000	µM	" "
$Km_{acotC4FFA}$	48000000	µM	" "
$Km_{acotC2FFA}$	13110000	µM	" "
Km_CoA	9	µM	[35]
$Keq_{acotC16}$	24000		[38]
$Keq_{acotC14}$	76000		[38]
$Keq_{acotC12}$	76000		[38]
$Keq_{acotC10}$	76000		[38]
Keq_{acotC8}	76000		[38]
Keq_{acotC6}	76000		[38]
Keq_{acotC4}	3000000		[38]
Keq_{acotC2}	570000		[38]
$Keq_{acotHBC}$	430000		[38]
$Keq_{acotHMG}$	17000		[38]
ACS			
sf_{acsC16}	0.91		[39]
sf_{acsC14}	0.97		[39]
sf_{acsC12}	1		[39]
sf_{acsC10}	0.4		[39]
sf_{acsC8}	0.068		[39]
sf_{acsC6}	0.0031		[39]
sf_{acsC4}	0.00014		Extrapolated
$Km_{C12FFACYT}$	4.55	µM	[39]
$Km_{C10FFACYT}$	7.69	µM	[39]
$Km_{C8KFFACYT}$	11.1	µM	[39]
$Km_{C6FFACYT}$	20.8	µM	[39]
$Km_{C4FFACYT}$	75.1	µM	Extrapolated

Parameter	Value	unit	References
Km_{CoACYT}	0.53	µM	[40]
Km_{ATPCYT}	500	µM	[40]
Omega-oxidation			
sf_{woxC16}	0.01		[41]
sf_{woxC14}	0.01		[41]
sf_{woxC12}	0.05		[41]
sf_{woxC10}	0.22		[41]
sf_{woxC8}	0.38		[41]
sf_{woxC6}	8		[41]
sf_{woxC4}	0.01		[41]
$V_{\omega ox}$	1.46	µmol.min^{-1}.mgProtein^{-1}	Estimated based on [42–45]
$Km_{woxC16FFAMICR}$	20000	µM	[41]
$Km_{woxC14FFAMICR}$	20000	µM	[41]
$Km_{woxC12FFAMICR}$	3.6	µM	[41]
$Km_{woxC10FFAMICR}$	522	µM	[41]
$Km_{woxC8KFFAMICR}$	4861	µM	[41]
$Km_{woxC6FFAMICR}$	6825	µM	[41]
$Km_{woxC4FFAMICR}$	20000	µM	[41]
$Km_{woxNADPHMICR}$	37	µM	[46]
Transmembranal transport parameters			
k_{mc}	3	L.min^{-1}.mgProtein^{-1}	Estimated arbitrarily
k_{cmi}	3	L.min^{-1}.mgProtein^{-1}	" "
k_{mic}	3	L.min^{-1}.mgProtein^{-1}	" "
k_{eFFA}	1E-06	L.min^{-1}.mgProtein^{-1}	" "
k_{eCn}	1E-06	L.min^{-1}.mgProtein^{-1}	" "
$k_{eAcetoacetateMAT}$	1E-06	L.min^{-1}.mgProtein^{-1}	" "
$k_{eBetahydroxybutyrateMAT}$	1E-06	L.min^{-1}.mgProtein^{-1}	" "
k_{eDCA}	1E-06	L.min^{-1}.mgProtein^{-1}	" "
Boundary metabolites and cofactors			
CarCYT	200	µM	[1]
CoACYT	140	µM	[1]
CarMAT	950	µM	[1]
AcetylCoAMAT	70	µM	[1]
ETFMATt	0.77	µM	[1]
NADtMAT	250	µM	[1]
NADHMAT	16	µM	[1]
CoQtMAT	288	µM	[47]
CoQH2MAT	28	µM	[47]
ATPCYT	4900	µM	[48]
NADPHMICR	356	µM	[49]

Parameter	Value	unit	References
Conserved moieties			
CoAMATt	5000	µM	[1]
Compartment volumes			
VCYT	$2.2 \cdot 10^{-6}$	L·mgProtein^{-1}	[1]
VMAT	$1.8 \cdot 10^{-6}$	L·mgProtein^{-1}	[1]
VMICR	$1.0 \cdot 10^{-6}$	L·mgProtein^{-1}	Estimated based on [50]

CPT1 parameters used for Figure 6.

Parameter	Value	Reference value	unit
CPT1			
$sf_{cpt1C14}$	0.134	1.34	
$sf_{cpt1C12}$	0.193	1.93	
$sf_{cpt1C10}$	0.154	1.54	
sf_{cpt1C8}	0.083	0.83	
sf_{cpt1C6}	0.051	0.51	
sf_{cpt1C4}	0.025	0.25	
$Km_{cpt1C14AcylCoACYT}$	30800	30.8	µM
$Km_{cpt1C12AcylCoACYT}$	11000	11	µM
$Km_{cpt1C10AcylCoACYT}$	16700	16.7	µM
$Km_{cpt1C8AcylCoACYT}$	22900	22.9	µM
$Km_{cpt1C6AcylCoACYT}$	151500	151.5	µM
$Km_{cpt1C4AcylCoACYT}$	653500	653.5	µM

We used these to simulate the effect of reduced activity and affinity towards C14-C4 acyl-CoA substrates.

References

1. van Eunen K, Simons SMJ, Gerding A, Bleeker A, den Besten G, Touw CML, Houten SM, Groen BK, Krab K, Reijngoud DJ, Bakker BM. Biochemical Competition Makes Fatty-Acid β-Oxidation Vulnerable to Substrate Overload. PLoS Comput Biol. 2013;9(8):2–9.
2. Wolters JC, Ciapaite J, van Eunen K, Niezen-Koning KE, Matton A, Porte RJ, Horvatovich P, Bakker BM, Bischoff R, Permentier HP. Translational targeted proteomics profiling of mitochondrial energy metabolic pathways in mouse and human samples. Submitt to Publ. 2016;
3. Finocchiaro G, Colombo I, DiDonato S. Purification, characterization and partial amino acid sequences of carnitine palmitoyl-transferase from human liver. FEBS Lett. 1990;274(1–2):163–6.
4. Ramsay RR, Derrick JP, Friend AS, Tubbs PK. Purification and properties of the soluble carnitine palmitoyltransferase from bovine liver mitochondria. Biochem J. 1987 Jun 1;244(2):271–8.
5. Gilbert HF, Lennox BJ, Mossman CD, Carle WC. The relation of acyl transfer to the overall reaction of thiolase I from porcine heart. J Biol Chem. 1981;256(14):7371–7.
6. Wiśniewski JR, Vildhede A, Norén A, Artursson P. In-depth quantitative analysis and comparison of the human hepatocyte and hepatoma cell line HepG2 proteomes. J Proteomics. 2016;136:234–47.
7. BLOISI W, COLOMBO I, GARAVAGLIA B, GIARDINI R, FINOCCHIARO G, DIDONATO S. Purification and properties of carnitine acetyltransferase from human liver. Eur J Biochem.

1990;189(3):539–46.
8. Miyazawa S, Ozasa H, Osumi T, Hashimoto T. Purification and properties of carnitine octanoyltransferase and carnitine palmitoyltransferase from rat liver. J Biochem. 1983;94(2):529–42.
9. Aoyama T, Souri M, Ushikubo S, Kamijo T, Yamaguchi S, Kelley RI, Rhead WJ, Uetake K, Tanaka K, Hashimoto T. Purification of human very-long-chain acyl-coenzyme A dehydrogenase and characterization of its deficiency in seven patients. J Clin Invest. 1995;95(6):2465–73.
10. Nandy A, Kieweg V, Krautle FG, Vock P, Küchler B, Bross P, Kim JJP, Rasched I, Ghisla S. Medium-long-chain chimeric human acyl-CoA dehydrogenase: Medium- chain enzyme with the active center base arrangement of long- chain acyl-CoA dehydrogenase. Biochemistry. 1996;35(38):12402–11.
11. van Eunen K, Volker-Touw CML, Gerding A, Bleeker A, Wolters JC, van Rijt WJ, Martines ACMF, Niezen-Koning KE, Heiner RM, Permentier H, Groen AK, Reijngoud DJ, Derks TGJ, Bakker BM. Living on the edge: Substrate competition explains loss of robustness in mitochondrial fatty-acid oxidation disorders. BMC Biol. 2016;14(1):1–15.
12. Izai K, Uchida Y, Orii T, Yamamoto S, Hashimoto T. Novel fatty acid beta-oxidation enzymes in rat liver mitochondria. I. Purification and properties of very-long-chain acyl-coenzyme A dehydrogenase. J Biol Chem. 1992 Jan 15;267(2):1027–33.
13. Finocchiaro G, Ito M, Tanaka K. Purification and properties of short-chain acyl-CoA, medium-chain acyl-CoA, and isovaleryl-CoA dehydrogenases from human liver. Adv Neurol. 1988;48(17):221–30.
14. Kiema TR, Harijan RK, Strozyk M, Fukao T, Alexson SEH, Wierenga RK. The crystal structure of human mitochondrial 3-ketoacyl-CoA thiolase (T1): Insight into the reaction mechanism of its thiolase and thioesterase activities. Acta Crystallogr Sect D Biol Crystallogr. 2014;70(12):3212–25.
15. Staack H, Binstock JF, Schulz H. Purification and properties of a pig heart thiolase with broad chain length specificity and comparison of thiolases from pig heart and Escherichia coli. J Biol Chem. 1978;253(6):1827–31.
16. Miyazawa S, Furuta S, Osumi T, Hashimoto T, Ui N. Properties of peroxisomal 3-ketoacyl-coA thiolase from rat liver. J Biochem. 1981 Aug;90(2):511–9.
17. Ramsay RR, Steenkamp DJ, Husain M. Reactions of electron-transfer flavoprotein and electron-transfer flavoprotein: ubiquinone oxidoreductase. Biochem J. 1987;241:883–92.
18. Beckmann JD, Frerman FE. Electron-Transfer Flavoprotein-Ubiquinone Oxidoreductase from Pig Liver: Purification and Molecular, Redox, and Catalytic Properties. Biochemistry. 1985;24(15):3913–21.
19. Watmough NJ, Loehr JP, Drake SK, Frerman FE. Tryptophan fluorescence in electron-transfer flavoprotein:ubiquinone oxidoreductase: fluorescence quenching by a brominated pseudosubstrate. Biochemistry. 1991;30(5):1317–23.
20. Frerman FE. Reaction of electron-transfer flavoprotein ubiquinone oxidoreductase with the mitochondrial respiratory chain. BBA - Bioenerg. 1987;893(2):161–9.
21. Husain M, Stankovich MT, Fox BG. Measurement of the oxidation-reduction potentials for one-electron and two-electron reduction of electron-transfer flavoprotein from pig liver. Biochem J. 1984;219(3):1043–7.
22. Karp G. No Title [Internet]. Table 5.1 in Karp; Gerald; Cell and Molecular Biology; 5th Ed.; Wiley; 2008. 2008. Available from: http://hyperphysics.phy-astr.gsu.edu/hbase/Chemical/redoxp.html
23. Huth W, Dierich C, Oeynhausen V v., Seubert W. Multiple mitochondrial forms of acetoacetyl-CoA thiolase in rat liver: Possible regulatory role in ketogenesis. Biochem Biophys Res Commun. 1974;56(4):1069–77.

24. Middleton B. The oxoacyl-coenzyme A thiolases of animal tissues. Biochem J. 1973;132(4):717–30.
25. Reed WD, Clinkenbeard D, Lane MD. Molecular and catalytic properties of mitochondrial (ketogenic) 3-hydroxy-3-methylglutaryl coenzyme A synthase of liver. J Biol Chem. 1975;250(8):3117–23.
26. Lowe DM, Tubbs PK. 3-Hydroxy-3-methylglutaryl-coenzyme A synthase from ox liver. Purification, molecular and catalytic properties. Biochem J. 1985;227:591–9.
27. Keq HMGCS2.
28. Stegink LD, Coon MJ. Stereospecificity and other properties of highly purified beta-hydroxy-beta-methylglutaryl coenzyme A cleavage enzyme from bovine liver. J Biol Chem. 1968;243(20):5272–9.
29. Tuinstra RL, Wang CZ, Mitchell GA, Miziorko HM. Evaluation of 3-Hydroxy-3-methylglutaryl-Coenzyme A Lyase Arginine-41 as a Catalytic Residue: Use of Acetyldithio-Coenzyme A to Monitor Product Enolization. Biochemistry. 2004;43(18):5287–95.
30. Keq HMGCL.
31. Tucker BGA, Dawson AP. The Kinetics of Rat Liver and Heart Mitochondrial P-Hydroxybutyrate Dehydrogenase. 1979;179:579–81.
32. Zhao H, Martin BM, Bisoffi M, Dunaway-Mariano D. The Akt C-terminal modulator protein is an Acyl-CoA thioesterase of the hotdog-fold family. Biochemistry. 2009;48(24):5507–9.
33. Pagliarini DJ, Calvo SE, Chang B, Sheth SA, Vafai SB, Ong SE, Walford GA, Sugiana C, Boneh A, Chen WK, Hill DE, Vidal M, Evans JG, Thorburn DR, Carr SA, Mootha VK. A Mitochondrial Protein Compendium Elucidates Complex I Disease Biology. Cell. 2008;134(1):112–23.
34. Ellis JM, Bowman CE, Wolfgang MJ. Metabolic and Tissue-Specific Regulation of Acyl-CoA Metabolism. PLoS One. 2015;10(3).
35. Cao J, Xu H, Zhao H, Gong W, Dunaway-Mariano D. The mechanisms of human hotdog-fold thioesterase 2 (h0054HEM2) substrate recognition and catalysis illuminated by a structure and function based analysis. Biochemistry. 2009;48(6):1293–304.
36. Moffat C, Bhatia L, Nguyen T, Lynch P, Wang M, Wang D, Ilkayeva OR, Han X, Hirschey MD, Claypool SM, Seifert EL. Acyl-CoA thioesterase-2 facilitates mitochondrial fatty acid oxidation in the liver. J Lipid Res. 2014;55(12):2458–70.
37. Tillander V, Nordström EA, Reilly J, Strozyk M, Van Veldhoven PP, Hunt MC, Alexson SEH. Acyl-CoA thioesterase 9 (ACOT9) in mouse may provide a novel link between fatty acid and amino acid metabolism in mitochondria. Cell Mol Life Sci. 2014;71(5):933–48.
38. Flamholz A, Noor E, Bar-Even A, Milo R. EQuilibrator - The biochemical thermodynamics calculator. Nucleic Acids Res. 2012;40(D1):770–5.
39. Marcel YL, Suzue G. Kinetic Studies on the Specificity of Long Chain Acyl Coenzyme A Synthetase from Rat Liver Microsomes Kinetic Coenzyme Studies on the Specificity from Rat of Long Liver Chain Acyl A Synthetase Microsomes. J Biol Chem. 1972;247(21):4433–6.
40. Fujino T, Man-Jong K, Suzuku H, Iijima H, Yamamoto T. Molecular Characterization and Expression of Rat Acyl-CoA Synthetase 3. J Biol Chem. 1996;271(28):16748–52.
41. Gregersen N, Mortensen PB, Kølvraa S. On the biologic origin of C6-C10-dicarboxylic and C6-C10-omega-1- hydroxy monocarboxylic acids in human and rat with acyl-CoA dehydrogenation deficiencies: in vitro studies on the omega- and omega-1-oxidation of medium-chain (C6-C12) fatty acids in human . PediatrRes. 1983;17(10):828–34.
42. Kawashima H, Naganuma T, Kusunose E, Kono T, Yasumoto R, Sugimura K, Kishimoto T. Human fatty acid ω-hydroxylase, CYP4A11: Determination of complete genomic sequence and characterization of purified recombinant protein. Arch Biochem Biophys. 2000;378(2):333–9.
43. Hoch U, Zhang Z, Kroetz DL, Ortiz de Montellano PR. Structural determination of the substrate specificities and regioselectivities of the rat and human fatty acid omega-hydroxylases. Arch

Biochem Biophys. 2000;373(1):63–71.

44. Gainer J V., Bellamine A, Dawson EP, Womble KE, Grant SW, Wang Y, Cupples LA, Guo CY, Demissie S, O'Donnell CJ, Brown NJ, Waterman MR, Capdevila JH. Functional variant of CYP4A11 20-hydroxyeicosatetraenoic acid synthase is associated with essential hypertension. Circulation. 2005;111(1):63–9.
45. Dierks EA, Zhang Z, Johnson EF, De Ortiz Montellano PR. The catalytic site of cytochrome P4504A11 (CYP4A11) and its L131F mutant. J Biol Chem. 1998;273(36):23055–61.
46. Miura Y, Hisaki H, Ueta N. omega- and (omega--1)-hydroxylation of fatty acids by frog liver microsomes. Substrate specificity and other properties. Biochim Biophys Acta. 1978 Nov 22;531(2):149–57.
47. Yugi K. Dynamic Kinetic Modeling of Mitochondrial Energy Metabolism. E-Cell Syst Basic Concepts Appl. 2013;105–42.
48. Soboll S, Seitz HJ, Sies H, Ziegler B, Scholz R, Chemie P, Diusseldorf IDU, Dusseldorf D-. Effect of long-chain fatty acyl-CoA on mitochondrial and cytosolic ATP / ADP ratios in the intact liver cell. 2000;220(1984):371–6.
49. Tischler ME, Friedrichs D, Coll K, Williamson JR. Pyridine nucleotide distributions and enzyme mass action ratios in hepatocytes from fed and starved rats. Arch Biochem Biophys. 1977 Nov;184(1):222–36.
50. Alberts B, Johnson A, Lewis J, Raff M, Roberts K, Walter P. The Compartmentalization of Cells. In: Molecular Biology of the Cell. 5th ed. New York: Garland Science; 2002.

Supplementary figures and tables

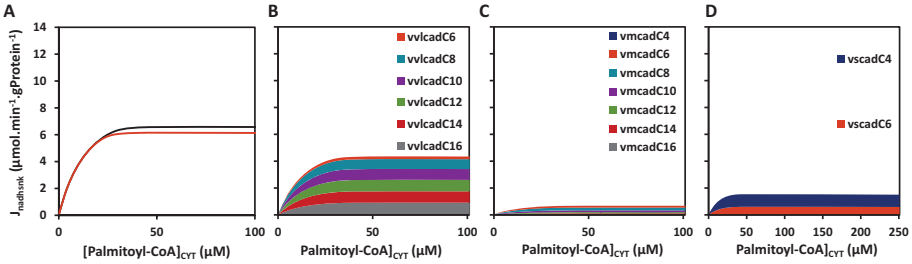

Supplementary figure S1, mFAO flux of WT and MCAD KO versions of the published fitted human isolated mFAO dynamic model [Eunen *et* al. 2016] (A) and steady-state fluxes through VLCAD (B), MCAD (C) and SCAD (D). Black: WT; Orange: MCAD KO.

Supplementary Table ST1. Flux and concentration control coefficients of the model as described in Supplementary Text ST1. The same model version (healthy, without any deficiencies) was used in Figure 2 in the main text. The control coeffients were calculated over the net NAD production flux (M/SCHAD plus MTP minus ketogenesis) , the consumption flux of palmitoyl-CoA by CPT1 (vCPT1 C16) and the CoASH concentration in the mitochondrial matrix (MAT).

	$J_{NAD\ production}$		$J_{CPT1C16}$		$[CoASH]_{MAT}$	
$[palmitoyl\text{-}CoA]_{CYT}$	**25 µM**	**100 µM**	**25 µM**	**100 µM**	**25 µM**	**100 µM**
Vcpt1	**0.59**	**0.00**	**0.61**	**0.06**	**-0.24**	**-1.11**
Vfcact	0.01	0.00	0.01	0.00	0.00	0.00
Vcpt2	0.01	0.00	0.01	0.00	0.00	-0.08
Vvlcad	0.01	0.01	0.00	0.01	0.00	-0.04
Vmcad	0.03	0.02	0.03	0.02	0.01	0.00
Vscad	0.01	0.00	0.01	0.00	0.00	0.05
Vcrot	0.00	0.00	0.00	0.00	0.00	0.00
Vmschad	0.00	0.00	0.00	0.00	0.00	0.00
Vmckat	0.03	0.01	0.02	0.01	0.02	0.06
Vmtp	0.00	0.00	0.00	0.00	0.00	0.00
Vacot	-0.04	0.00	-0.04	0.00	0.02	0.09
Vacat1	0.01	0.01	0.01	0.00	0.01	0.03
Vhmgcs2	0.00	0.00	0.00	0.00	0.00	0.00
Vhmgcl	0.00	0.00	0.00	0.00	0.00	0.00
Vbdh1	0.00	0.00	0.00	0.00	0.00	0.00
Vfetfqo	**0.35**	**0.95**	**0.33**	**0.88**	**0.18**	**0.98**
kmc	0.00	0.00	0.00	0.00	0.00	0.00
Vacs	-0.01	0.00	-0.01	0.00	0.01	0.02
kcmi	0.00	0.00	0.00	0.00	0.00	0.00
Vwox	0.01	0.00	0.01	0.00	0.00	-0.01
kmic	0.00	0.00	0.00	0.00	0.00	0.00
keFFA	0.01	0.00	0.01	0.00	0.00	-0.01
keCn	0.00	0.00	0.00	0.01	0.00	0.01
keDCA	0.00	0.00	0.00	0.00	0.00	0.00
keAcetoacetateMAT	0.00	0.00	0.00	0.00	0.00	0.01
keBetahydroxybutyrateMAT	0.00	-0.01	0.00	0.00	0.00	0.00

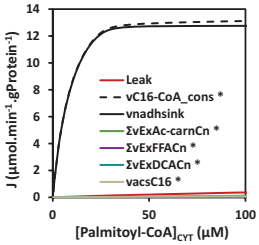

Supplementary Figure S2. Net NADH production fluxes in the mitochondria (vnadhsink), palmitoyl-CoA consumption flux in nadh production equivalents, leakage of incompletely oxidized intermediate metabolites ("Leak") expressed in nadh production equivalents and reaction rates which the leakage consists of, namely acyl-carnitine export (ΣvExAc-carnCn), free fatty acid export (ΣvFFACn), dicarboxylic acid export (ΣvDCACn) and ACS-catalyzed return of palmitoyl-CoA to its constant pool (also in nadh production equivalents).

Supplementary Table ST2. Flux control coefficients of model with ACS knockdown to 1% of its reference value

	$J_{NAD\ production}$		$J_{CPT1C16}$		$[CoASH]_{MAT}$	
$[palmitoyl\text{-}CoA]_{CYT}$	**25 µM**	**100 µM**	**25 µM**	**100 µM**	**25 µM**	**100 µM**
Vcpt1	**0.31**	0.00	**0.34**	0.07	**-0.35**	**-1.04**
Vfcact	0.00	0.00	0.00	0.00	0.00	0.00
Vcpt2	0.01	0.00	0.01	0.00	-0.01	-0.09
Vvlcad	0.02	0.01	0.01	0.01	0.00	-0.09
Vmcad	0.03	0.02	0.03	0.02	0.01	0.02
Vscad	0.00	0.00	0.01	0.00	0.01	0.06
Vcrot	0.00	0.00	0.00	0.00	0.00	0.00
Vmschad	0.00	0.00	0.00	0.00	0.00	0.01
Vmckat	0.02	0.01	0.02	0.01	0.03	0.08
Vmtp	0.00	0.00	0.00	0.00	0.00	0.00
Vacot	0.00	0.00	0.00	0.02	0.01	0.04
Vacat1	0.01	0.01	0.00	0.00	0.01	0.04
Vhmgcs2	0.00	0.00	0.00	0.00	0.00	0.00
Vhmgcl	0.00	0.00	0.00	0.00	0.00	0.00
Vbdh1	0.00	0.00	0.00	0.00	0.00	0.00
Vfetfqo	**0.60**	**0.96**	**0.56**	**0.86**	**0.30**	**0.95**
kmc	0.00	0.00	0.00	0.00	0.00	0.00
Vacs	0.00	0.00	0.00	0.00	0.00	0.00
kcmi	0.00	0.00	0.00	0.00	0.00	0.00
Vwox	0.00	0.00	0.00	0.00	0.00	0.00
kmic	0.00	0.00	0.00	0.00	0	0.00
keFFA	0.00	0.00	0.00	0.00	0.00	0.00
keCn	0.00	0.00	0.00	0.01	0.00	0.01
keDCA	0.00	0.00	0	0	0	0.00
keAcetoacetateMAT	0.00	0.00	0.00	0.00	0.00	0.01
keBetahydroxybutyrateMAT	0.00	-0.01	0.00	0.00	0.00	0.00

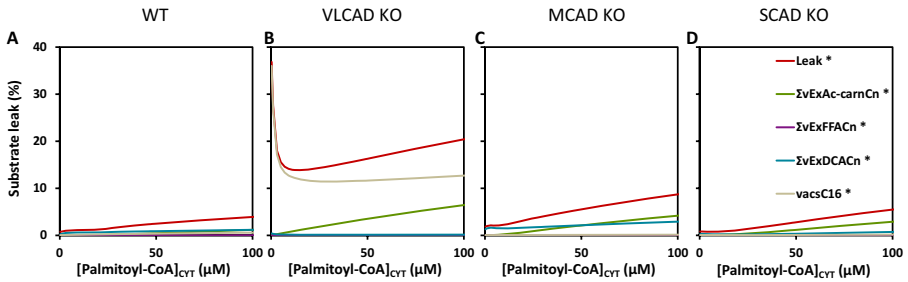

Supplementary Figure S3. Simulation results of the model with ACS-knockdown to 1% of its reference value. Panels **A-D** display substrate leakage rates as percentage of palmitoyl-CoA consumption flux expressed in NADH production equivalents for the WT (**A**), VLCAD KO (**B**), MCAD KO (**C**) and SCAD KO (**D**) version of the model.

Supplementary Table ST3. Flux control coefficients of WT model with C16-specific CPT1

	$J_{NAD\ production}$		$J_{CPT1C16}$		$[CoASH]_{MAT}$	
$[palmitoyl\text{-}CoA]_{CYT}$	**25 µM**	**100 µM**	**25 µM**	**100 µM**	**25 µM**	**100 µM**
Vcpt1	**1.02**	**1.01**	**1.02**	**1.00**	**-0.02**	**-0.11**
Vfcact	0.01	0.00	0.00	0.00	0.00	0.00
Vcpt2	0.00	0.00	0.00	0.00	0.00	0.00
Vvlcad	0.01	0.00	0.01	0.00	0.00	0.00
Vmcad	0.16	0.17	0.16	0.17	0.00	-0.01
Vscad	-0.02	-0.04	-0.02	-0.04	0.00	0.01
Vcrot	0.00	0.00	0.00	0.00	0.00	0.00
Vmschad	0.00	0.00	0.00	0.00	0.00	0.00
Vmckat	0.08	0.05	0.08	0.05	0.01	0.01
Vmtp	0.00	0.01	0.00	0.01	0.00	0.00
Vacot	**-0.33**	**-0.36**	**-0.33**	**-0.36**	0.01	0.04
Vacat1	0.01	0.01	0.01	0.01	0.00	0.00
Vhmgcs2	0.00	0.00	0.00	0.00	0.00	0.00
Vhmgcl	0.00	0.00	0.00	0.00	0.00	0.00
Vbdh1	0.00	0.00	0.00	0.00	0.00	0.00
Vfetfqo	0.04	0.16	0.04	0.17	0.01	0.06
kmc	0.00	0.00	0.00	0.00	0.00	0.00
Vacs	-0.05	-0.04	-0.05	-0.04	0.00	0.00
kcmi	0.00	0.00	0.00	0.00	0.00	0.00
Vwox	0.04	0.03	0.04	0.03	0.00	0.00
kmic	0.00	0.00	0.00	0.00	0.00	0.00
keFFA	0.01	0.00	0.01	0.00	0.00	0.00
keCn	0.00	0.00	0.00	0.00	0.00	0.00
keDCA	0.00	0.00	0.00	0.00	0.00	0.00
keAcetoacetateMAT	0.00	0.01	0.00	0.01	0.00	0.00
keBetahydroxybutyrateMAT	0.00	0.00	0.00	0.00	0.00	0.00

In this model version the K_m values for C4-C16 acyl-CoA substrates were increased, while the corresponding V_{max} values were decreased.The parameters of the C16-specific CPT1 are given in Supplementary Text ST1.

Supplementary table ST4. Total C16-C4 CoA ester concentrations in ACAD KO en WT models with C16-specific CPT1.

	Reference model			Model with C16-specific CPT1		
Model	J_{mFAO}	$[R\text{-}CoA]_{mat}$	$[R\text{-}CoA]_{cyt}$	J_{mFAO}	$[R\text{-}CoA]_{mat}$	$[R\text{-}CoA]_{cyt}$
WT	12.8	1495	179	11.5	112	189932
VLCAD KO	4.1	1611	5	4.1	1611	9620
MCAD KO	8.0	2368	207	4.9	48	680116
SCAD KO	11.6	2586	1290	11.6	2505	676935

R denotes C16-C4 chain lengths,so $[R\text{-}CoA]_{MAT}$ the total CoA ester concentration in the matrix and $[R\text{-}CoA]_{cyt}$ the total CoA ester concentration in the cytosol. The parameters of the C16-specific CPT1 are given in Supplementary Text ST1.

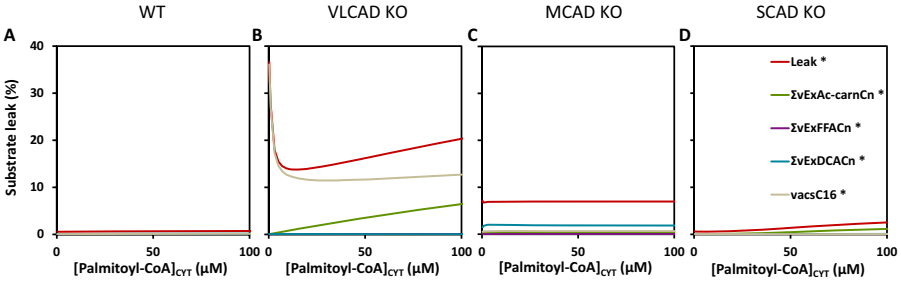

Supplementary Figure S4. Simulation results of the extended model with a more C16-specific CPT1, *i.e.* a CPT1 which is less sensitive C14-C4 chain length reactants, for WT and single-enzyme ACAD KO. Panels **A-D** displays substrate leakage rates as percentage of palmitoyl-CoA consumption flux expressed in NADH production equivalents for the WT (**A**), VLCAD KO (**B**), MCAD KO (**C**) and SCAD KO (**D**) version of the model.

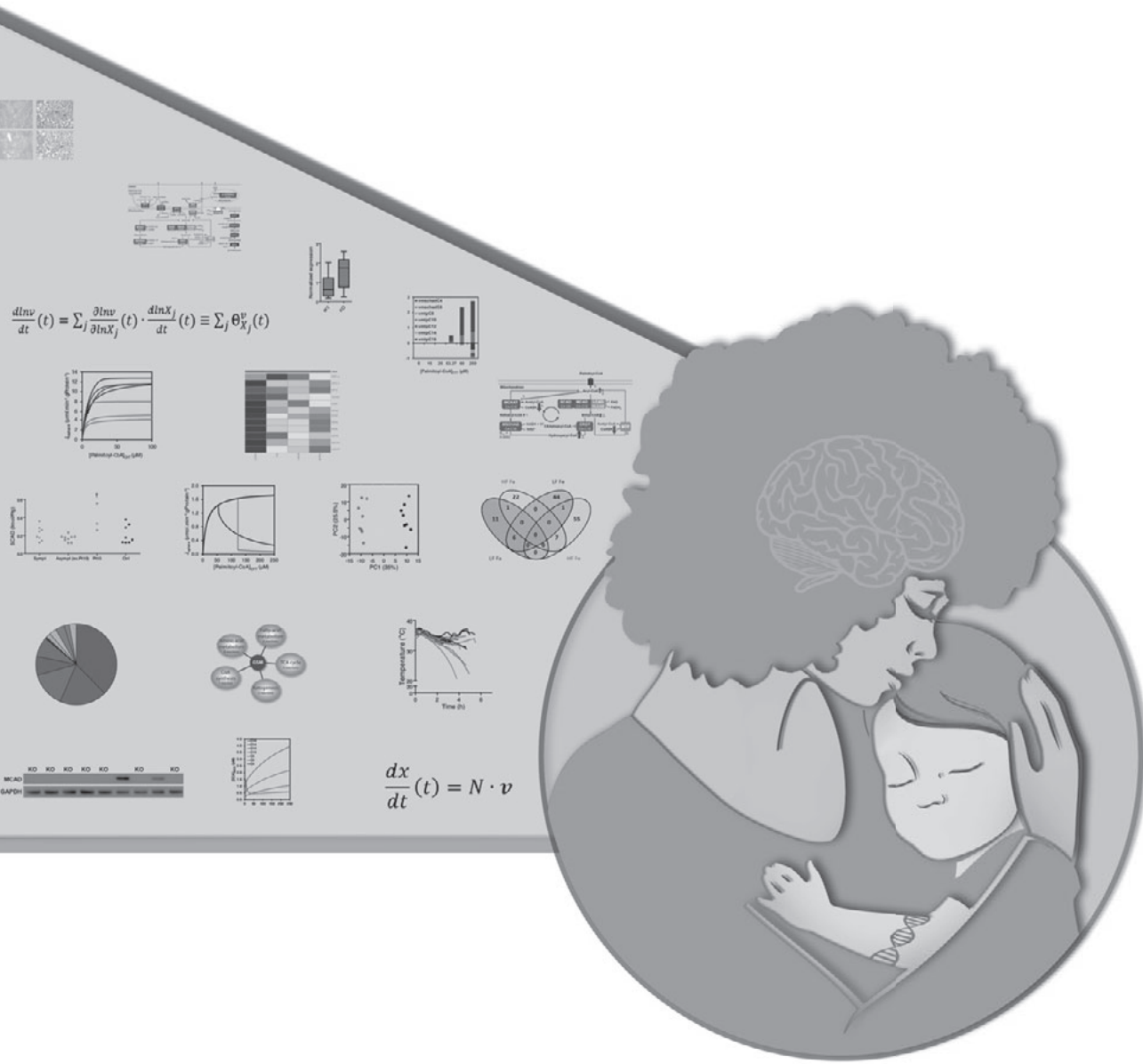
$\frac{dlnv}{dt}(t) = \sum_j \frac{\partial lnv}{\partial lnX_j}(t) \cdot \frac{dlnX_j}{dt}(t) \equiv \sum_j \theta^v_{X_j}(t)$
KO KO KO KO KO KO KO
MCAD
GAPDH
$\frac{dx}{dt}(t) = N \cdot v$